A thesis for the degree of Doctor of Philosophy

A Study on High-Reliable Wireless Video Transmission Scheme

Division of Media Network Technologies
Graduate School of Information Science and Technology
Hokkaido University, Japan

Hirokazu Tanaka

September, 2015

Contents

List of Figures

List of Tables

Chapter 1

Introduction

1.1 Background

The rapid growth of wireless and mobile technologies is creating demands for various multimedia applications and services at all times and from anywhere. One new that is very much in demand is that of video content. A main reason for this is that the number of smartphones and PCs has been steeply rising, allowing people to easily enjoy video multimedia services. Video coding technology has previously been focused on broadcast, movie, video-on-demand via Internet, etc.[1]-[2]. Therefore, video coding schemes have been extensively studied for obtaining higher coding efficiency in order to transmit higher resolution video contents over a limited bandwidth channel and international standardization bodies have created new video codec standards in response to this requirement, e.g., MPEG-2, MPEG-4, H.264 and H.265 [3]-[6].

Recently, we have had more opportunities to utilize video multimedia applications for not only broadcast but also other use cases, e.g. extreme environment and healthcare applications [7],[8]-[10]. The background of this trend comes from the fact that real-time video transmission can be easily realized using a small video camera and codec device including a mobile terminal. Due to recent advances in LSI technology, the processing ability of software video codecs has becomes sufficiently high to expand the use cases of video transmission systems. In many such applications, wireless video transmission systems employ mobile ad-hoc networks and their technical requirements are

different from those of broadcast systems [11]-[13]. In these systems, error resiliency against the loss or erasure of video streams is more important. This implies that high-reliable (dependable or error robust) video transmission is required in parallel with high resolution video transmission.

For the high-reliable wireless transmission systems, Multi-carrier Code Division Multiple Access (CDMA) has become a promising candidate for future wireless multimedia communications including high-reliable wireless transmission systems because of its robustness to frequency-selective fading and its flexibility in handling multiple data rates [14]-[20]. Multi-carrier CDMA is intended to exploit the advantages of both Orthogonal Frequency Division Multiplexing (OFDM) [21] and CDMA, and can be mainly divided into two categories: spreading in the frequency domain (MC-CDMA) and spreading in the time domain (MC-DS-CDMA). The longer symbol interval in OFDM greatly eases the problem of acquiring synchronization of the spreading code in the receiver. Additionally, it can achieve high data rate transmission with protection against frequency selective fading and eliminate the need for RAKE combing [14],[18]-[20]. However, Multi-carrier CDMA systems suffers from performance degradation by a high peak to average power ratio (PAPR) and multi-path fading [18]-[26].

1.2. Motivation of the Research

As a solution for achieving the new technical requirements for video transmission described in the previous section, this thesis presents two kinds of new proposals: one is for a spatial and temporal error concealment (EC) method that is suitable for the packet loss channel and the other is for a new wireless transmission scheme that can transmit a highly error-protected video stream over error-prone channels and with high transmission efficiency (high frequency utilization efficiency). Figure 1.1 shows the structure of the considered mobile multimedia communication system. A video input and an audio input are encoded at each encoder. These encoded and control data are input into a multiplexing module. At this module, the input sequence is encapsulated into multiplexing packets (MUX packets) and each packet adds a multiplexing packet header and Cyclic Redundancy Check (CRC) for the detection of the packet header. For video multimedia transmission, MPEG-2 TS is often applied for the multiplexing scheme. The MUX packet is fed into a channel coding module and the packet is error-protected by an error control code.

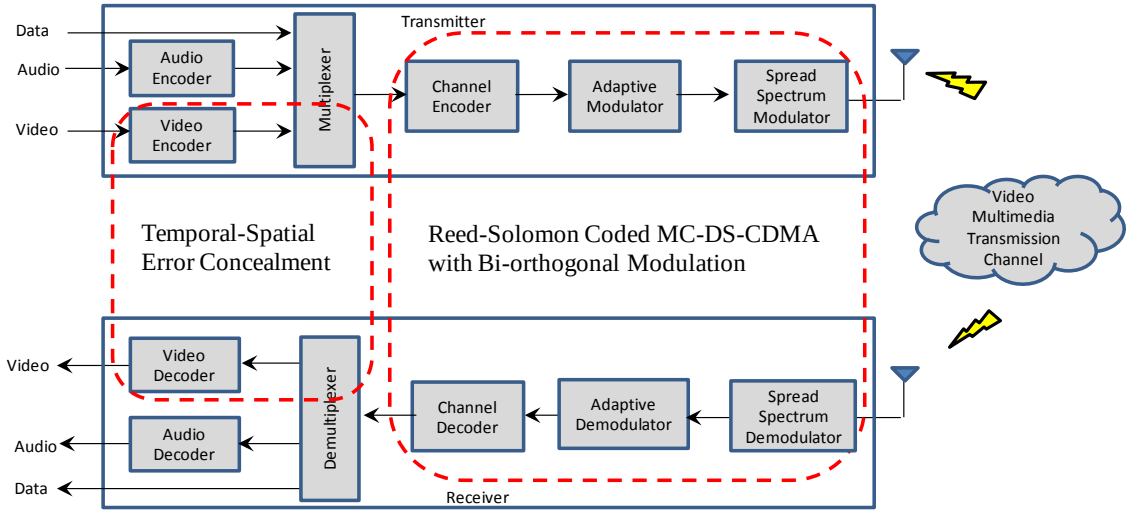

Fig. 1.1 System structure and coverage area of this thesis

This encoded packet is then modulated by an adaptive modulator. After modulation, the signal is spread by a spreading code and transmitted into the channel. The receiver operates the inverse procedures of the transmitter. In this figure, the coverage areas of the above two proposals are shown. The spatial and temporal EC method indicates a solution in the upper layer and the new wireless transmission scheme, Reed-Solomon (RS) coded MC-DS-CDMA with bi-orthogonal modulation covers the lower layer.

1.2.1 Spatial and Temporal Error Concealment Method

Conventional video communication systems widely adopt video coding schemes using discrete cosine transform (DCT) coding and motion estimation and compensation (ME/MC) [3]-[6],[27]. The discrete wavelet transform (DWT) has become increasingly popular: this has advantages in reducing block artifacts, especially at a low bit rate and giving efficient scalability [28]-[29]. In 3D DWT video coding, the video encoder can produce energy-condensed wavelet coefficients and a scalable bit stream [28],[30]. Thus, in error-prone wireless networks, packet losses that can cause serious degradation of video quality are inevitable [31]. Therefore, it is important to develop error-resilient coding methods to minimize visual quality degradation [32],[33]. One of the most prominent error-resilient coding methods is grouping or packetization methods for video sequences without extra redundant information [34]-[39]. In addition to error-resilient coding, EC at the decoder is also an efficient method for compensating visual quality [40]-[42].

In [43]-[44], we proposed a 3D DWT video coding employing dispersive grouping (DG) and a two-step EC method. The first step involves recovering lost coefficients in the spatiotemporal lowest-frequency sub-band using those duplicated coefficients transmitted in dispersively grouped bit-streams and the second step is recovering lost coefficients using interpolation methods. In these papers, the interpolation methods are applied in each frame (only intra-frame). Note that higher efficiency of the interpolation can be obtained by utilizing temporal similarities.

1.2.2 Error Control Coding for MC-DS-CDMA with Bi-orthogonal Modulation

Among the various Multi-carrier CDMA schemes, hybrid schemes of bi-orthogonal keying and Multi-carrier CDMA have been proposed [23],[46]-[47]. In this scheme, the input sequence of a

bi-orthogonal modulator is defined as the following two types: $n-1$ bits out of n input bits (called code-selection bits) and the remaining 1 bit (called a sign bit). The code-selection bits select a Hadamard code word as a spreading code and the sign bit is transmitted after spread by the selected Hadamard code word. An advantage of this modulation scheme is that the bandwidth efficiency is higher than that of the orthogonal modulation, e.g., an n-bit input sequence is spread into 2^n bits by orthogonal modulation and 2^{n-1} bits by bi-orthogonal modulation,. This indicates that the multi-user capacity can be doubled on the same process gain condition. In [47], it is shown that the PAPR and bit error rate (BER) performances over multi-path fading channels can be reduced by using a cyclically shifted Chu sequence. Applying error correction codes is also an important approach to combat against these performance degradations. Traditionally, employing convolutional codes to mobile communication systems has been studied [48]-[52]. However, when adopting error correction codes to MC-DS-CDMA with a bi-orthogonal modulation scheme, the following points should be considered:

- A two-step demodulation is performed at each bi-orthogonal demodulator. The code-selection bits are detected and then a decision for the corresponding sign bit is applied using the above detected code selection bits. Therefore, if the code-selection bits can be protected sufficiently, the sign bit error can also be reduced sufficiently.
- Since the code-selection bit sequence consists of $n-1$ bits, employing a symbol error correcting (burst error correcting) code is more efficient for encoding code-selection bits. This implies that employing a non-binary code is more suitable than employing a binary code.
- Since several bi-orthogonal modulators are allocated in parallel, the number of encoders and decoders should be minimized. Additionally, their implementation complexity should be as low as possible.

Additionally, if an efficient error control coding can be adopted based on the above conditions, we can further consider increasing the transmission efficiency of the sign bit by using multi-level modulation. This allows the system to realize high speed video multimedia transmission. When applying multi-level modulation, an additional efficient error control coding needs to be considered.

1.3. Organization of this Thesis

A layout of this thesis and how the chapters link together are provided in Fig. 1.2. The remainder of this thesis is organized as follows.

In Chapter 2, an enhanced spatial and temporal EC method is proposed to achieve higher performance in packet loss networks. This is an extension of our previous studies and offers the challenge of achieving higher EC performance. To improve the EC performance, the following modifications are made;

- In addition to the spatial EC method in [43],[45], a temporal EC method is employed. Compared with the conventional two-step EC method, this temporal EC requires no additional procedure at the encoder. Only the decoding procedure is modified,
- In the temporal EC method, the structural similarity (SSIM) index is used for inter-group of pictures (GOP) EC and the minimum mean square error (MMSE) is used for intra-GOP EC. The SSIM index was proposed for predicting human preferences in evaluating image quality [53]-[54]. Since it can be assumed that human visual perception is highly adapted for extracting structural information from a scene, the SSIM index can provide efficient visual quality-prediction performance.

In Chapter 3, the MC-DS-CDMA with a bi-orthogonal modulation system is explained and an efficient error correction coding scheme suitable for this system is proposed. An RS code [55]-[56] is employed for encoding the code-selection bits. The advantages of the RS code are as follows: 1) It is a widely used symbol error correction (non-binary) code and high correction abilities can be expected: 2) this code is capable of parallel processing, enabling ease high-speed implementations: and 3) each code-selection bit of the bi-orthogonal modulators can be assigned as an RS code symbol. This implies that the code-selection errors for all subcarriers can be corrected by a single error correction code. As for the sign bit error protection, no error correction code is adopted. Instead of employing an error correction code, the detection algorithm at the bi-orthogonal demodulator is modified. As a basic analysis of the proposed scheme, BPSK is assumed for the sign bit modulation.

In Chapter 4, to realize a high-speed mobile communication system of the type that should be necessary for real-time video multimedia transmission, a multi-level modulation (e.g., MPSK and MQAM) scheme is desired in that it achieves higher frequency utilization efficiency. In applying multi-level modulations to multi-carrier systems, Adaptive Modulation and Coding (AMC) has been

extensively studied [57]-[58]. As an extension to a high-speed mobile communication system, a Generalized Symbol-rate-increased (GSRI) Adaptive Trellis Coded Modulation (ATCM) scheme applied to RS-coded MC-CDMA with bi-orthogonal keying (hereinafter called proposed scheme) is adopted. The GSRI TCM that we have proposed allows bandwidth-expansion ratio to be varied aiming at an optimization between complexity of the system design complexity and the coding gain improvement [59]. This scheme can arbitrarily set the bandwidth-expansion ratio, keeping higher coding gain than the conventional TCM scheme. Since a Pragmatic TCM [60] is used, the modulation scheme can be easily changed according to the channel conditions. As for MC-CDMA systems, the performance degradation by Peak-to-Average Power Ratio (PAPR) due to a non-linear amplifier is another important problem to be solved. Since GSRI TCM does not expand the number of the modulation scheme, the performance degradation due to the nonlinearity of the amplifier can be reduced [60]-[61]. For applying GSRI TCM to the MC-CDMA with bi-orthogonal keying, the following modifications are employed.

- Instead of MQAM schemes, we assume the application of MPSK schemes for reducing the performance degradation by a nonlinear amplifier [60]-[61].
- To reduce the performance degradation over multi-path fading channels, an inter-subcarrier interleaving is employed.

It is clarified that there is a tradeoff between BER and throughput for the proposed scheme and the RS-coded MC-CDMA with bi-orthogonal keying employing the conventional Pragmatic TCM.

The results of this thesis are summarized in the conclusions presented in Chapter 5.

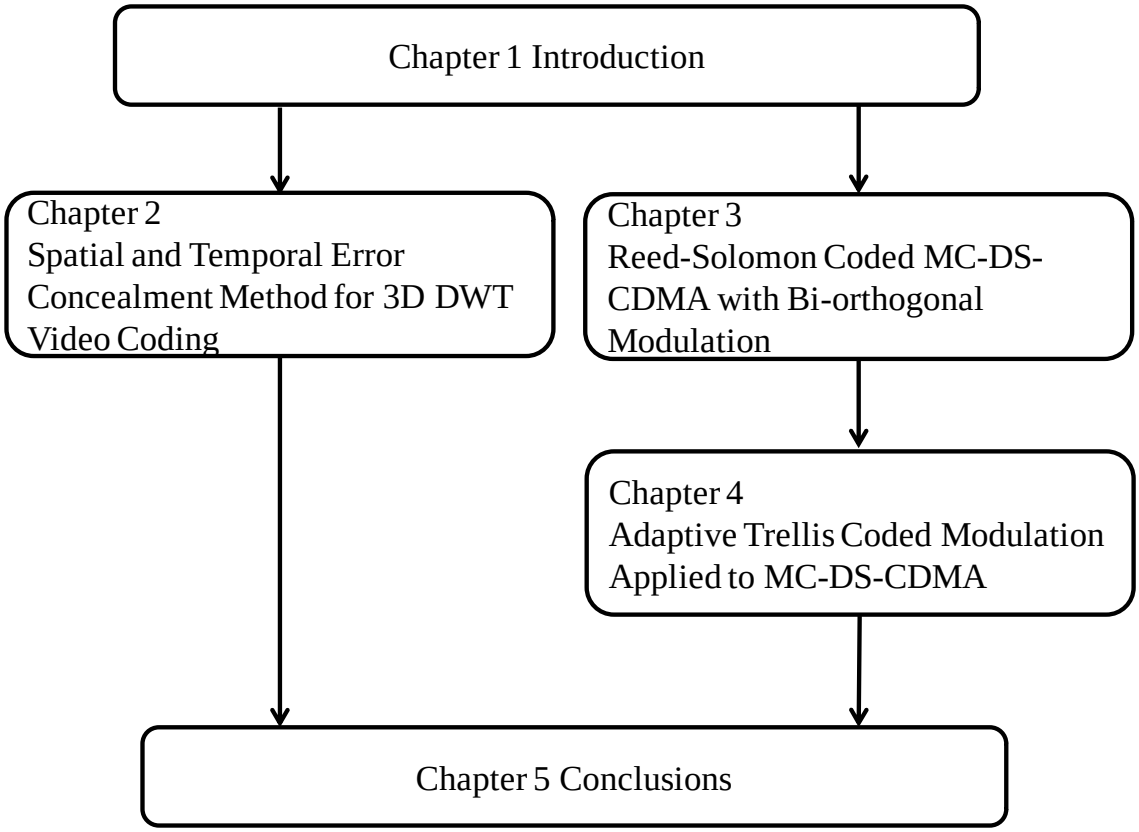

Fig. 1.2 Organization of this thesis

Chapter 2

Spatial and Temporal Error Concealment Method for 3D DWT Video Coding

2.1. Introduction

A new spatial and temporal EC method for three-dimensional discrete wavelet transform (3D DWT) video coding is analyzed. 3D DWT video coding employing dispersive grouping (DG) and two-step EC is an efficient method in a packet loss channel [43], [45]. In the two-step EC method, the interpolations are only spatially applied: however, a higher efficiency of the interpolation can be expected by utilizing spatial and temporal similarities. In this chapter, an enhanced spatial and temporal EC method for achieving higher EC performance in packet loss networks is proposed. In the temporal EC method, a structural similarity (SSIM) index is employed for inter-group of pictures (GOP) EC and minimum mean square error (MMSE) is used for intra-GOP EC.

2.2 System Description

Figure 2.1 shows the system model. The transmitter consists of a video encoder, audio encoder,

multiplexer and modulator. The video coding is focused on analysis. Audio coding is not described. The input video stream is encoded at the 3D DWT encoder. The structure of the 3D DWT video encoder is illustrated in Fig. 2.2. In this figure, the input video sequence is divided into groups of successive frames for forming a GOP. These frames are provided by the 3D DWT module and a wavelet transform cube is generated by spatial DWT and temporal DWT.

An example of a wavelet transform process is explained in Fig. 2.3. This figure illustrates a case of a 4×4 pixel frame with GOP size = 4. Each of the four input video frames is spatially wavelet-transformed first. In this figure, the transformation process for Frame #1 is illustrated. One-dimensional DWT is performed for each row (Step1). Then 1D DWT is performed for each column as Step2. Step3 gives 1D DWT processes for the all rows and columns in the LL part. The same spatial wavelet transform process is performed for the other frames (Frames #2, 3 and 4). After finishing the spatial wavelet transform, a temporal wavelet transform is performed. This time, 1D DWT is performed in the direction of the time axis. In a temporal DWT process, pixels located at the same position in each transformed frame of the spatial wavelet are selected.

The wavelet coefficient $w(u,v,s)$ given by the 3D DWT decomposition process is dispersively divided into several groups (DGs are constructed) in order to obtain error-resilient bit-streams. The dispersive grouping algorithm is a remainder function for generating a group index using unique indices – the location of frame (u,v) and the frame number (s) - of a video sequence [45].

Each DG is quantized at the quantized module and the spatiotemporal low-frequency sub-band duplication information is applied in order to provide enhanced concealment capabilities [45].

Then, each group is entropy-coded at the entropy-coding module and input to the multiplexer. At the multiplexer, the transmission packets for the MPEG-2 Transport Stream (TS) format [44] are generated. As described in [45], the packetized elementary stream (PES) packets are created from the bit stream and then encapsulated inside the TS payload. Each TS payload generates a TS packet (TSP) by adding a 4 byte TS header. In Fig.2.1, the TSPs are sent through the modulator and transmitted to the receiver. At the receiver, demodulation is performed and video TSPs are extracted with DGs being re-constructed at the demultiplexer. The re-constructed DGs are inputted into a 3D DWT video decoder. At the decoder, decoding and EC are performed through the following seteps:

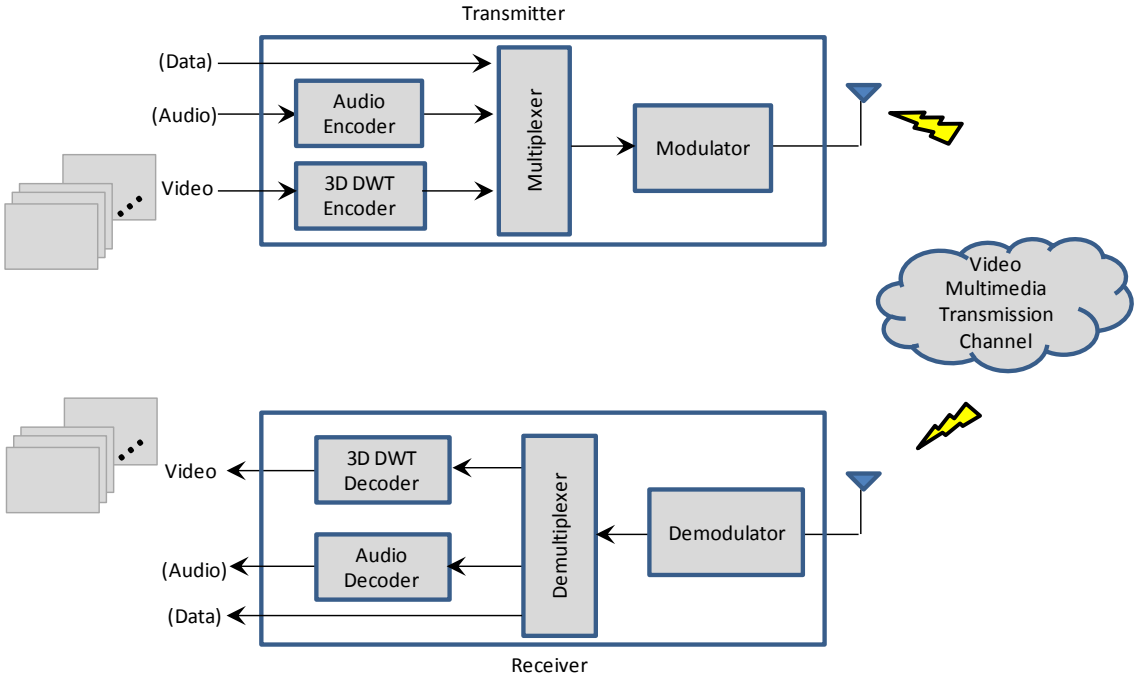

Fig. 2.1 System model

1. Inverse packetization and checking the erroneous coefficients of the received signal,
2. Replacement method of EC
3. Inverse dispersive grouping
4. Temporal EC
5. Inverse temporal decomposition
6. Spatial EC
7. Inverse spatial decomposition

The next section explains the EC methods in detail.

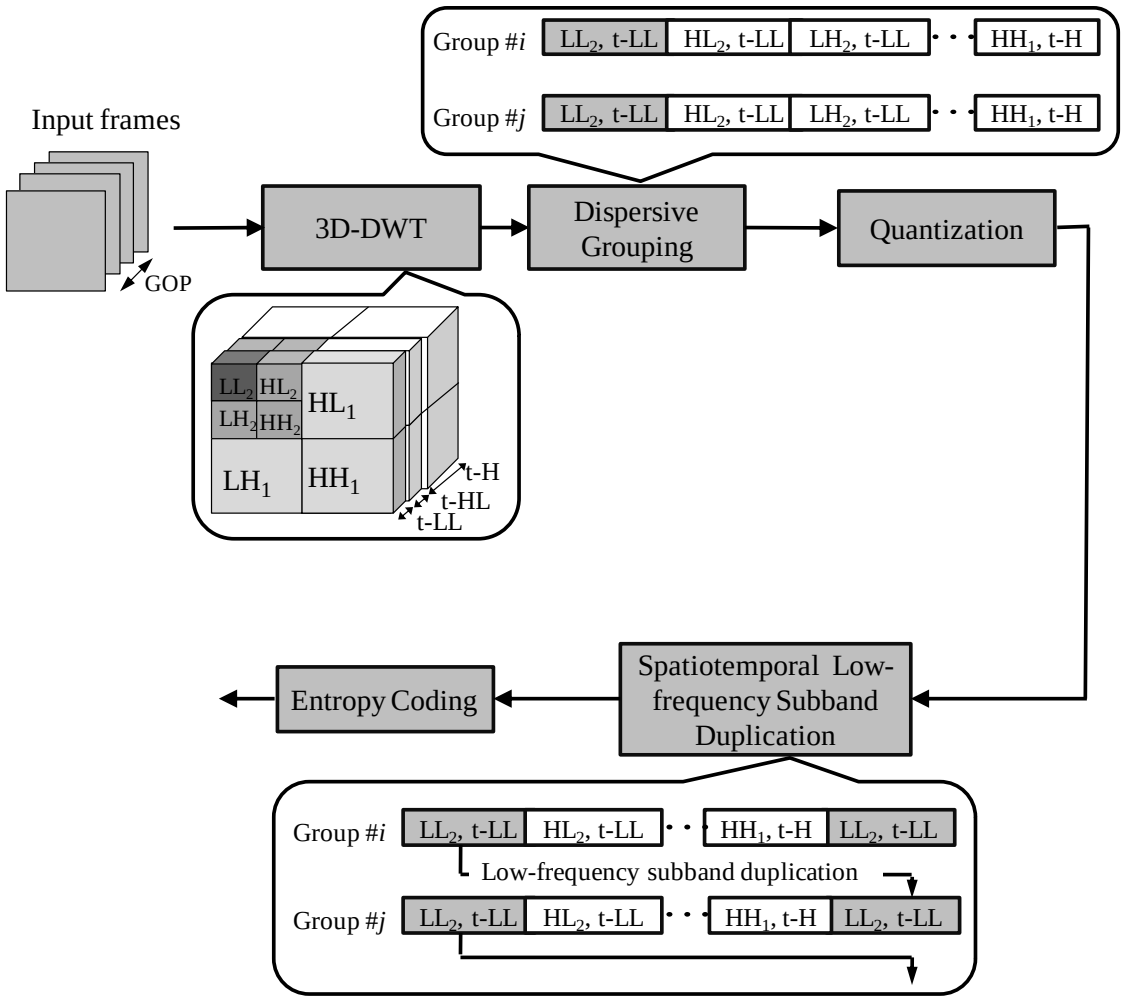

Fig. 2.2 Structure of the 3D DWT encoder

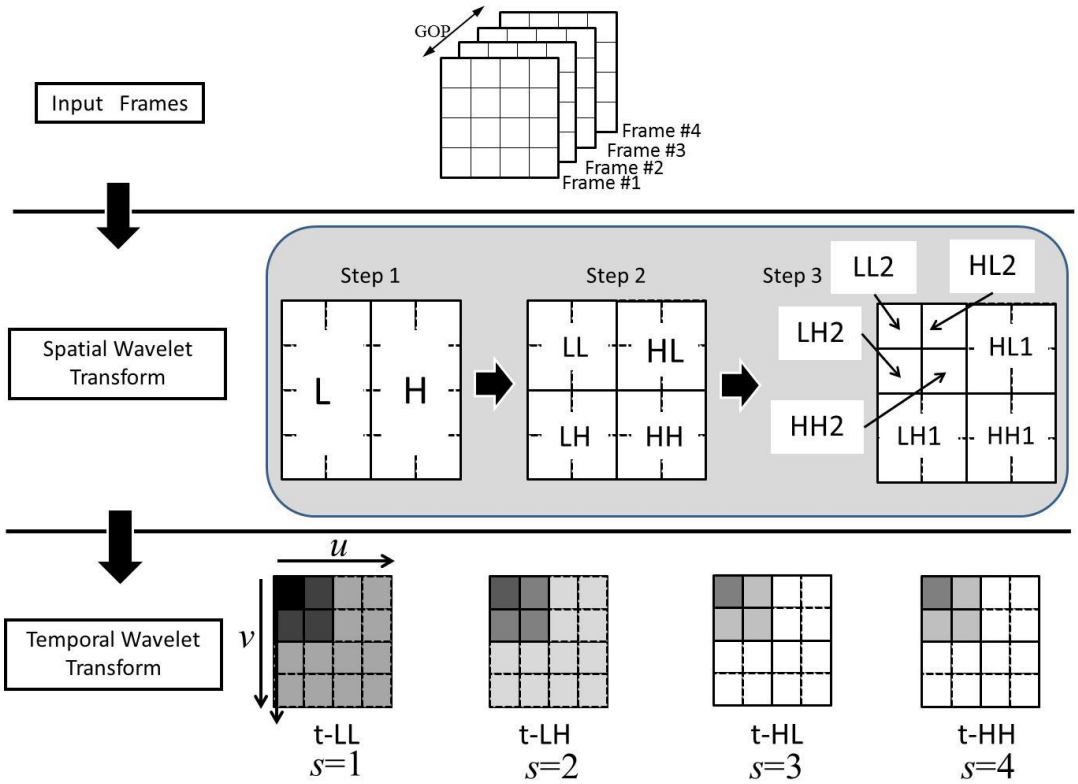

Fig. 2.3 Example of 3D DWT (GOP size =4)

2.3 Proposed Error Concealment

2.3.1 Replacement Method

Decoding failures or missing coefficients propagate to the related spatiotemporal coefficients in a GOP frame period in the wavelet domain. Therefore, the EC method is applied before the inverse 3D DWT processing operation. The decoder first recovers the detected loss coefficient by replacement procedure with its duplicated coefficient as follows:

$$\hat{w}_i(u,v,s) = \begin{cases} w'_j(u,v,s) & if\ available \\ 0 & if\ \ lost \end{cases}, \tag{2.1}$$

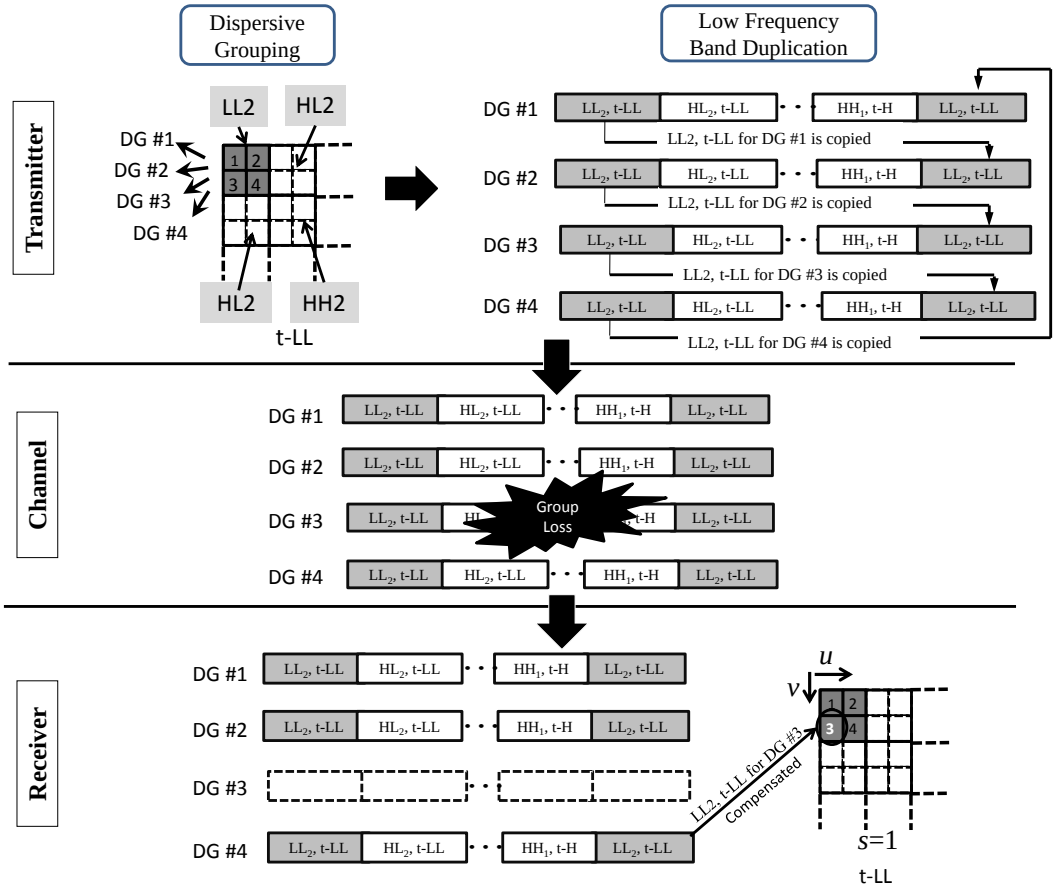

Fig. 2.4 Example of the replacement method

where $\hat{w}_i(u,v,s)$ denotes an estimated value of the lost coefficient of the *i*-th group, in which *u* and *v* denote the coordinates and *s* is the frame index. $w_j(u,v,s)$ is a duplication coefficient that is transmitted by including the *j*th group.

Figure 2.4 shows an example of the above procedure. Assuming that the lowest sub-band coefficients are dispersively divided into four groups, 4 DGs are generated. Among the four DGs, DG #3 is corrupted in the channel and a group loss takes place. In this case, the lowest sub-band coefficients in the DG #3 ($\hat{w}_3(1,2,1)$) cannot be provided with the decoder. However, since DG #4 has a copy of the coefficients ($w'_4(1,2,1)$), this loss can be compensated.

The replacement based concealment method can expect remarkable error recovery performance by using multiple transmission effects. However, the lost coefficients of the low-frequency sub-band

are unable to recover perfectly when both the original and duplicated coefficients are lost. This procedure is basically the same as EC I in [45].

2.3.2 Temporal Error Concealment

An SSIM index is a method for measuring the similarity between two frames. Generally, the similarity of the lowest sub-band frames between neighboring GOPs is high. In such a condition, interpolation weighting factors based on PSNR or MSE are difficult to represent accurate visual quality. Since the SSIM index can reflect perceptual distortions, it can represent the visual quality accurately [62]-[64]. The SSIM index between *s*-th frame and *k*-th frame is defined as follows [53]:

$$SSIM(s,k) = \frac{(2\mu_s\mu_k + C_1)(2\sigma_{sk} + C_2)}{(\mu_s^2 + \mu_k^2 + C_1)(\sigma_s^2 + \sigma_k^2 + C_2)}, \tag{2.2}$$

where μ_s and μ_k represent the mean values of the *s*-th frame and *k*-th frames, respectively, σ_s and σ_k are the standard deviations of each of frame, and σ_{sk} is the covariance of the two frames. The constants C_1 and C_2 are two small positive constants and calculated as follows:

$$C_1 = (K_1 L)^2,\ C_2 = (K_2 L)^2, \tag{2.3}$$

where L is the dynamic range of pixel values (e.g., 255 for 8-bit image), and K_1 and K_2 are small constants for avoiding instability. The maximum SSIM value, 1, is achieved in the case of two identical sets of data.

In Fig. 2.5, the proposed method is adopted into the inter-GOP based temporal EC method for temporal low-frequency sub-band (t-LLL). The concealed value of the *s*-th frame in the current GOP (k = 0) $\hat{w}_{LB}(u,v,s)$ is calculated as as follows:

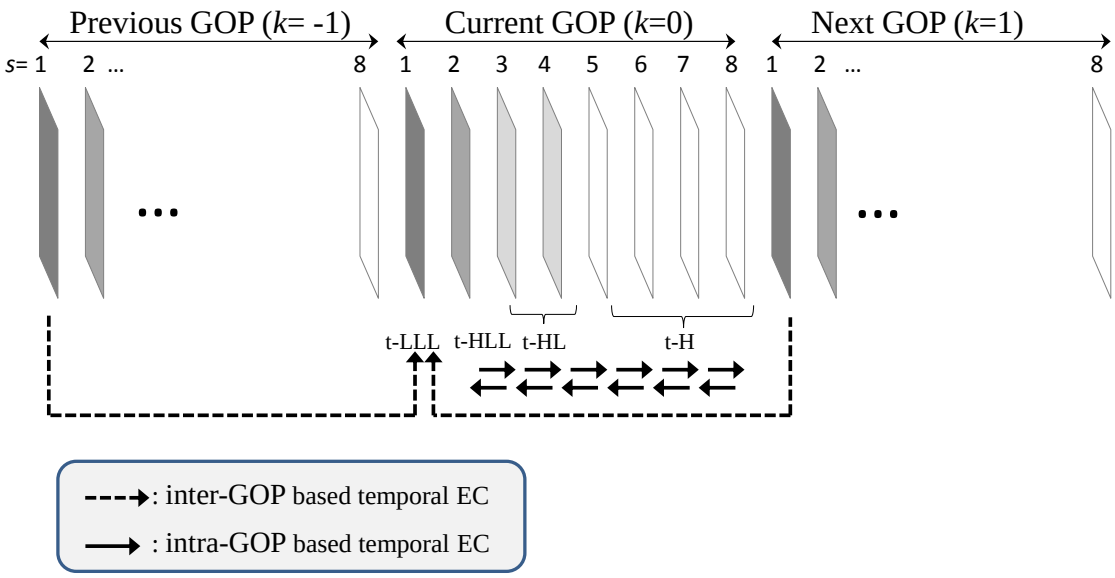

Fig. 2.5 Structure of the proposed temporal EC method (GOP length = 8, decomposition level = 3)

$$\hat{w}_{LB}(u,v,s) = \frac{1}{2(2r+1)^2} \cdot \frac{\sum_{i=-r}^{r}\sum_{j=-r}^{r}\sum_{k=-1,k\neq 0}^{1}\alpha_{s,L_G k}\, w(u+i, v+j, s+L_G k)}{\sum_{i=-r}^{r}\sum_{j=-r}^{r}\sum_{k=-1,k\neq 0}^{1}\alpha_{s,L_G k}} \quad , \tag{2.4}$$

where $\hat{w}_{LB}(u,v,s)$ is an estimated value for the erroneous coefficient of the low-frequency sub-band, L_G is the length of one GOP period, r is a reference area index of the concealing processing, and $\alpha_{sL_G k}$ is a weighting factor between the current frame s and the reference frame $L_G k$. The weighting factor for the inter-GOP based temporal EC method is derived by the SSIM index value as follows:

$$\begin{aligned}\alpha_{s,L_G k} &= SSIM_{LB}(s, L_G k) \\ &= \frac{(2\mu_s \mu_{L_G k} + C_1)(2\sigma_{sL_G k} + C_2)}{(\mu_s^2 + \mu_{L_G k}^2 + C_1)(\sigma_s^2 + \sigma_{L_G k}^2 + C_2)},\end{aligned} \tag{2.5}$$

where μ_s and σ_s are given by

$$\mu_s = \frac{1}{M_{LL} N_{LL}} \sum_{i=1}^{M_{LL}} \sum_{j=1}^{N_{LL}} w(i, j, s), \tag{2.6}$$

and

$$\sigma_s^2 = \frac{1}{M_{LL} N_{LL}} \sum_{i=1}^{M_{LL}} \sum_{j=1}^{N_{LL}} (w(i, j, s) - \mu_s)^2, \tag{2.7}$$

with M_{LL} and N_{LL} being the width and height of the spatiotemporal low-frequency sub-band, respectively. In eq. (2.5), $\mu_{s+L_G k}$ and $\sigma_{s+L_G k}$ are also calculated with (2.6) and (2.7). The covariance of the current frame s and reference frame, $L_G k$, is given by

$$\sigma_{sL_G k} = \frac{1}{M_{LL} N_{LL}} \cdot \sum_{i=1}^{M_{LL}} \sum_{j=1}^{N_{LL}} (w(i, j, s) - \mu_s)(w(i, j, L_G k) - \mu_{L_G k}) . \tag{2.8}$$

Along with intra-frame based temporal EC shown in Fig. 2.5, temporal high-frequency sub-band frames are concealed using adjacent reference frames as follows;

$$\hat{w}_{HB}(u,v,s) = \frac{1}{2(2r+1)^2} \cdot \frac{\sum_{i=-r}^{r}\sum_{j=-r}^{r}\sum_{k=-1,k\neq 0}^{1}\beta_{s,k}(i,j)w(u+i,v+j,s+k)}{\sum_{i=-r}^{r}\sum_{j=-r}^{r}\sum_{k=-1,k\neq 0}^{1}\beta_{s,k}(j,j)}, \tag{2.9}$$

where w_{HB} is an estimated value of the erroneous wavelet coefficient and $\beta_{s,k}(i,j)$ is a weighting factor of the reference coefficient. The weighting factor of each neighboring coefficient is derived by the MMSE algorithm.

A set of temporal adjacent reference coefficients can be expressed as follows:

$$\mathrm{T} = \begin{bmatrix} w(u-r,v-r,s+k) & \dots & w(u-r,v+r,s+k) \\ \vdots & \ddots & \vdots \\ w(u+r,v-r,s+k) & \cdots & w(u+r,v+r,s+k) \end{bmatrix}. \tag{2.10}$$

The weighting factor in each reference coefficient is chosen according to the dominant correlation by using the MMSE algorithm. We estimate the weighting factors as follows:

$$\beta_{s,k}(i,j) = \mathrm{R}_{\mathrm{HE}_{i,j}} \mathrm{R}^{-1}_{\mathrm{E}_{i,j}\mathrm{E}_{i,j}}, \tag{2.11}$$

where H is the set of surrounding coefficients of a lost coefficient $w(u,v,s)$ and can be expressed as follows:

$$\mathrm{H} = \begin{bmatrix} w(u-r,v-r,s) & \dots & w(u-r,v+r,s) \\ \vdots & \ddots & \vdots \\ w(u+r,v-r,s+k) & \cdots & w(u+r,v+r,s) \end{bmatrix}. \tag{2.12}$$

The set of surrounding coefficients of the reference coefficient $w(u+i, v+j, s+k)$ is expressed as follows:

$$\mathrm{E}_{i,j} = \begin{bmatrix} w(u+i-r, v+j-r, s+k) & \dots & w(u+i-r, v+j+r, s+k) \\ \vdots & \ddots & \vdots \\ w(u+i+r, v+j-r, s+k) & \cdots & w(u+i+r, v+j+r, s+k) \end{bmatrix}. \tag{2.13}$$

In eq. (2.14), $R_{E_{i,j}E_{i,j}}$ is the auto-correlation matrix of $E_{i,j}$ and $R_{HE_{i,j}}$ is the cross-correlation matrix of H and $E_{i,j}$. In practical implementation, an approximation of $\mathrm{R}_{\mathrm{E}_{i,j}\mathrm{E}_{i,j}}$ and $\mathrm{R}_{\mathrm{H}\mathrm{E}_{i,j}}$ can be calculated from the empirical data as

$$\mathrm{R}_{\mathrm{E}_{i,j}\mathrm{E}_{i,j}} = \mathrm{E}\left[\mathrm{E}_{i,j}\mathrm{E}_{i,j}^{T}\right], \quad R_{\mathrm{HE}_{i,j}} = \mathrm{E}\left[\mathrm{HE}_{i,j}^{T}\right]. \tag{2.14}$$

Finally, we set minimum and maximum thresholds of the weighting factor in order to obtain a reliable estimated value because a zero-correlation result causes an inappropriate value. The ranges of the estimated values $(Th_{\min}, Th_{\max})$ are defined as follows:

$$\beta_{s,k}(i,j) = \begin{cases} Th_{\mathrm{min}} & \beta_{s,k}(i,j) < Th_{\mathrm{min}} \\ \beta_{s,k}(i,j) & Th_{\mathrm{min}} < \beta_{s,k}(i,j) < Th_{\mathrm{max}} \\ Th_{\mathrm{max}} & \beta_{s,k}(i,j) > Th_{\mathrm{max}} \end{cases} \tag{2.15}$$

2.3.3 Spatial Error Concealment

The proposed spatial EC is based on statistical models for video frame coefficients by training on the neighboring coefficients in the current frame. A set of spatial reference wavelet coefficients for the spatial EC method can be expressed as follows:

$$\mathrm{S} = \begin{bmatrix} w(u-r, v-r, s) & \dots & w(u-r, v+r, s) \\ \vdots & \ddots & \vdots \\ w(u+r, v-r, s) & \cdots & w(u+r, v+r, s) \end{bmatrix}. \tag{2.16}$$

The equation of spatial EC method is expressed as

$$\hat{w}_{SP}(u,v,s) = \frac{1}{(2r+1)^2} \cdot \frac{\sum_{i=-r}^{r}\sum_{j=-r}^{r}\gamma_s(i,j)w(u+i,v+j,s)}{\sum_{i=-r}^{r}\sum_{j=-r}^{r}\gamma_s(i,j)}, \tag{2.17}$$

where $\gamma_s(i,j)$ is a weighting factor for the spatial EC method.

The set of surrounding coefficient matrices for each reference coefficient $w(u+i,v+j,s+k)$ is given as follows:

$$\mathrm{E}_{i,j} = \begin{bmatrix} w(u+i-r,v+j-r,s) & \dots & w(u+i-r,v+j+r,s) \\ \vdots & \ddots & \vdots \\ w(u+i+r,v+j-r,s) & \cdots & w(u+i+r,v+j+r,s) \end{bmatrix}. \tag{2.18}$$

The weighting factor $\gamma_s(i,j)$ of the spatial EC method is given by

$$\gamma_s(i,j) = \mathrm{R}_{SE_{i,j}}\mathrm{R}^{-1}_{E_{i,j}E_{i,j}}. \tag{2.19}$$

This factor is obtained using eqs. (2.14), (2.15) and (2.19). A large area is needed to calculate a weighting factor for the low-frequency sub-band which has a high variance. However, it is not easy to calculate an accurate weighting factor despite the increasing of area index, *r*. Therefore, a bilinear interpolation method is used to conceal the loss coefficient in the low-frequency sub-band as shown in eq. (2.4).

2.4 Performance Evaluation

In this section, the performance of the proposed EC method is evaluated through simulations. The simulation parameters are given in Table 2.1. To evaluate the basic EC performance, the channel is assumed to be a random error model. From the viewpoint of the basic performance evaluations, it is efficient to perform the evaluation over a system-independent channel model. Furthermore, mobile

Table 2.1 Simulation parameters.

Video sequence type	YUV 4:2:0
Frame rate	30 frames/s
Spatial DWT filter	Daubechies 9/7
Temporal DWT filter	Haar
Spatial decomposition level (s_lev)	3
The length of GOP frames (L_G)	8, 16, 32 frames
Temporal decomposition level (t_lev)	4
Number of dispersive groups (N_D)	4
Packet loss patterns	Random
Weighting factor threshold $(Th_{\min}, Th_{\max})$	(0.01, 100)
The reference coefficients area index (r)	1

communication systems usually support interleavers for randomizing the channel errors. If the interleaver works sufficiently well, the channel condition can be assumed as a random error channel.

The PSNR vs. Packet Loss Rate (PLR) performance is evaluated in Fig. 2.6. The example video sequences are selected as a relatively slow-motion *Highway* sequence and a relatively fast-motion *Football* sequence. The proposed method is compared with the two-step EC method. In this simulation, the GOP size is selected to be as 16 frames. For *Highway* sequence, the proposed method achieves better performance than the two-step EC method. This implies that the temporal EC is effectively working in a slow-motion sequence. In the slow motion video sequences, the similarity between the reference frames is high effectiveness can be expected for the temporal EC. On the other hand, the improvement in the proposed method is marginal in the case of the *Footbal* sequence. In the fast-motion sequences, the similarity between the reference frames is relatively low and the temporal EC performs less effectively.

Figure 2.7 shows the PSNR vs. GOP size at a PLR of 10%. The evaluated video sequences are also *Football* as a relatively fast-motion sequence and *Highway* as a relatively slow-motion sequence. In this figure, it is observed that the performance improvement of the proposed method is attractive for various GOP sizes in the case of *Highway*. It is also indicated that the temporal EC works effectively in a slow-motion sequence. In the case of *Football*, the performance improvement of the

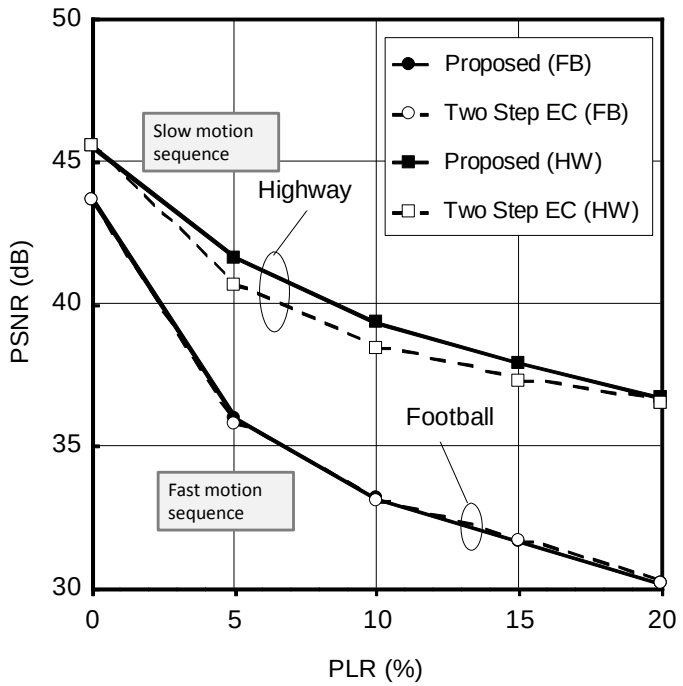

Fig. 2.6 Packet loss rate vs. PSNR for *Football* and *Highway* (GOP =16)

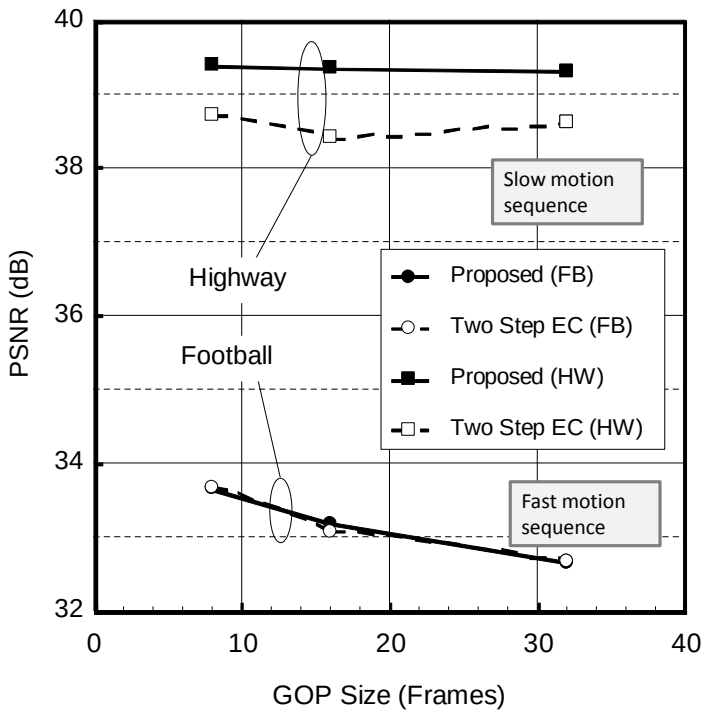

Fig. 2.7 GOP size vs. PSNR for *Football* and *Highway* (PLR =10%)

Table 2.2 PSNR performance (PLR= 12.5%)

Video sequence	Two-step EC method	Proposed method	Improvement
Football	31.87dB	32.11dB	0.24dB
Foreman	32.26dB	33.17dB	0.91dB
Paris	28.78dB	31.02dB	2.24dB
Highway	37.55dB	38.56dB	1.01dB
Mobile	26.49dB	27.65dB	1.16dB
Bridge	33.38dB	34.70dB	1.32dB

proposed method is marginal for various GOP sizes.

The performance of the proposed method is evaluated for various video sequences. The average PSNR performance results of the proposed method and the two-step EC method at a PLR of 12.5% are shown in Table 2.2. For all of the video sequences, the proposed method has the best PSNR performance compared with the other methods. It is indicating that the proposed method can obtain the best EC ability. Among the video sequences in this table, it can also be said that relatively slow motion video sequences (e.g., *Highwa*y and *Bridge*) perform better than the fast-motion ones (e.g., *Football* sequence). This implies that the temporal EC for the slow motion sequences is more effective than that for the fast motion video sequences. The above evaluations show that the proposed method remarkably improves PSNR performance when video sequences are relatively slow. In order to compare visual quality, typical examples of decoded frames for *Highway* sequence at the PLR of 12.5% are shown in Fig. 2.8. For reference, the experimental results of the following error concealment methods are presented in addition to the conventional methods: Bilinear EC [37], Adaptive MAP EC [41] and GMRF model based EC [42]. In this figure, we can see there are still erroneous coefficients (black dots) in Fig. 2.8 (b), (c) and (d). In Fig. 2.8 (e), it shows that the conventional Two-step EC method attains better improvements compared with the above three conventional methods. In Fig. 2.8 (f), the proposed method achieves the best visual quality. Comparing Fig. 2.8 (e) and (f), it is observed that blurry areas on the road are reduced. It is because the proposed method utilizes the temporal EC in addition to the spatial EC.

As for the increase in the implementation complexity due to the temporal EC method, the transmitter has no additional functionality. Only the receiver increases the implementation for the

additional EC method. The main additional parts are a buffer for the previous and next GOPs and logics for SSIM interpolation and MMSE interpolation. To perform inter-GOP interpolations, at least three GOPs (the previous, current and next GOPs) have to be stored in the decoder buffer. This requires a buffer that is three times larger than that in conventional methods. The calculations for SSIM interpolation are inclined to be more complex than that for MMSE interpolation. Optimizing the implementation design, there may be a possibility of sharing the MMSE logic for temporal EC and that for spatial EC.

2.5 Conclusion

In this chapter, a spatial and temporal EC methods for 3D DWT video coding are proposed and the PSNR performances are evaluated using simulations in a packet-transmission channel. Based on the two-step EC method, the proposed method employs an extended temporal EC. There are two main ideas behind this temporal EC. One is referencing inter-GOP frames for the lowest sub-band frames and intra-GOP frames for the higher sub-band frames and the other is employing the SSIM indicator for inter-GOP frames. The proposed method can first recover packet errors using a spatial EC method with spatiotemporal low-frequency sub-band duplication information and then the video decoder can recover erroneous video frames from spatiotemporal adjacent coefficients.

The simulation results revealed that the proposed EC method performs better than the two-step EC method. It was also shown that the proposed method achieves remarkable improvement for relatively slow-motion video sequences. An efficient method for relatively fast motion video sequences should be further investigated. Employing motion compensation is one technique to be considered. It should also be compared from the viewpoints of performance and implementation complexity.

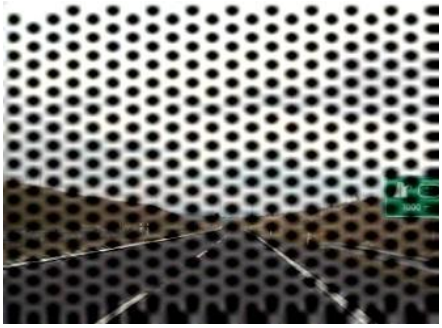

(a) Erroneous frame

(b) Bilinear EC

(c) Adaptive MAP EC

(d) GMRF EC

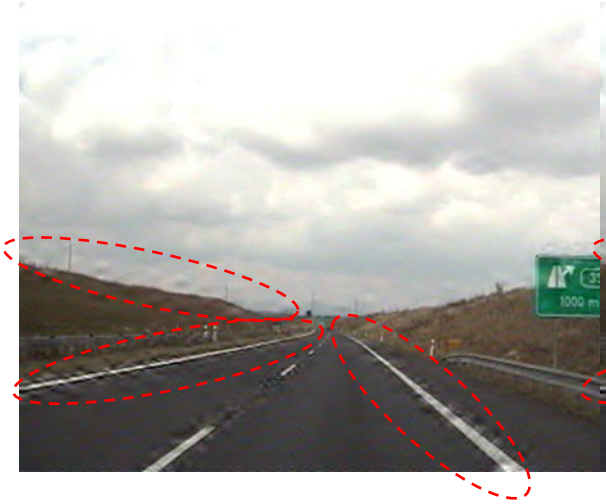

(e) Two-step EC

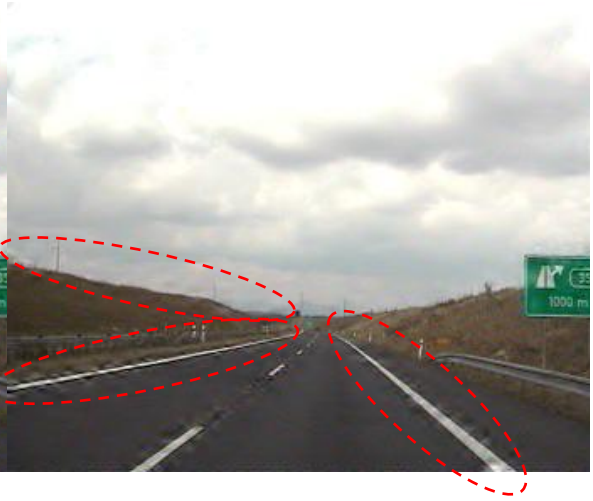

(f) Proposed EC

Fig. 2.8 Reconstructed sample frame of the *Highway* sequence in a 12.5% packet loss rate environment.

Chapter 3

Reed-Solomon Coded MC-DS-CDMA with Bi-orthogonal Modulation

3.1. Introduction

In this chapter, an error correction scheme suitable for an MC-DS-CDMA system with bi-orthogonal modulation is presented. The input sequence of a bi-orthogonal modulator consists of an $n-1$ bit code-selection bit sequence and 1 bit sign bit sequence. To apply an efficient error correction code, the following points should be considered: (1) if the code-selection bits can be protected sufficiently, the sign bit error can also be reduced sufficiently, (2) since a code-selection bit sequence consists of $n-1$ bits, employing a symbol error correcting code is more effective for encoding code selection bits, and (3) the complexity of the error correction encoder and decoder implementations should be minimal. Based on these conditions, we propose employing a Reed-Solomon (RS) code for encoding the code-selection bits and no error correction code for the sign bit. Additionally, the detection algorithm at the bi-orthogonal demodulator is modified to compensate for degradations of the sign BER performance. The performance in an Additive White Gaussian Noise (AWGN) channel is evaluated by both theoretical analysis and computer simulations. The performance evaluations by simulations on multi-path fading channels are also shown.

3.2. System Description

3.2.1 Transmitter Structure

The transmitter structure of the proposed scheme is given in Fig. 3.1(a). The incoming binary bits are serial-to-parallel converted into $kq+n$ parallel bit streams, where k is the number of the input sequences sent to the RS encoder and q is the number of bits in each input sequence. These k input sequences, $i=(i_0,\ldots,i_{k-1})$, are fed to the (n,k)RS encoder over GF(2^q). The encoded symbols $b_0,\ldots,b_{n-1}$ are inputted into n bi-orthogonal modulators and each modulator selects an orthogonal code. Here we can define the coding rate of the transmitter, *r*, as follows:

$$r=\frac{kq+n}{(q+1)n} \quad . \tag{3.1}$$

The detailed scheme of the bi-orthogonal modulator is shown in Fig. 1(b). The orthogonal code used here is the Hadamard code. When the *q* bits b_j ($j=0,\ldots,n-1$) are fed into the modulator, one of the *h* Hadamard codewords is selected according to the bit combination of b_j and the selected codeword is outputted as c_j. In this figure, $h=2^q$ $(=n+1)$ is assumed. On the other hand, *n* parallel 1-bit signals, a_j ($j=0,\ldots,n-1$), are modulated by BPSK. The modulated signal u_j ($j=0,\ldots,n-1$) is expressed as follows:

$$u_j=\begin{cases}+1 & ;a_j=0\\ -1 & ;a_j=1\end{cases}. \tag{3.2}$$

Then, $u_0\cdots u_{n-1}$ are spread by the selected Hadamard codewords, $c_0\cdots c_{n-1}$. The modulated sequences $s_0,\ldots,s_{n-1}$ are fed into the *N*-point IFFT. Since the number of IFFT points is generally set to 2^ℓ (ℓ is a positive integer), *N* is defined as *n*+1 (in this case, 2^q), which means an additional 0 padding carrier is assumed to be inserted. The output of the IFFT signal, $X(t)$, is expressed as

$$X(t)=\frac{1}{\sqrt{N}}\sum_{m=0}^{N-1}s_m\cdot e^{j2\pi m\Delta ft}\ , \tag{3.3}$$

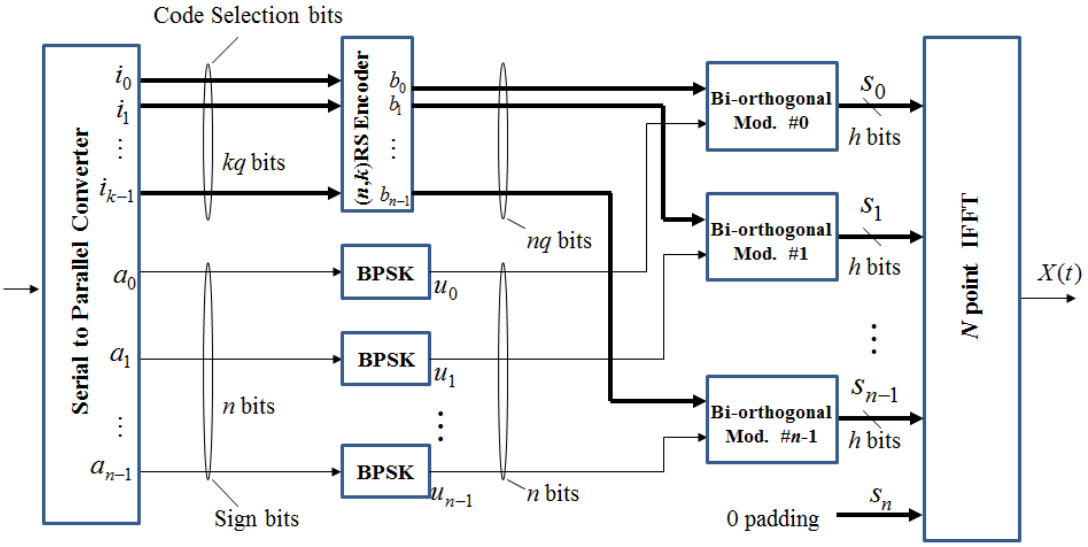

(a)

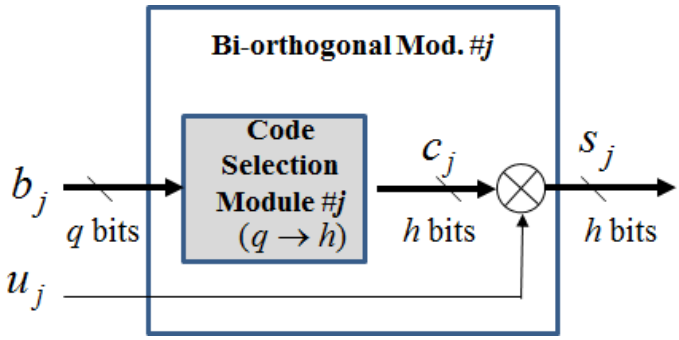

(b)

Fig. 3.1 (a) Transmitter structure of the proposed scheme
(b) Bi-orthogonal modulator of the transmitter

where $\Delta f = 1/T_s$ and T_s denotes a modulated symbol (hereinafter called an OFDM symbol) period.

An example is shown in Figs. 3.2(a) and (b). This example is a case where $q = 3$, $h = 2^q = 8$, $n = 2^q - 1 = 7$, $k = 3$ and $N = 2^q = 8$. The incoming binary bits are serial-to-parallel converted into 10 parallel sequences. Among these sequences, $i_0, \cdots, i_2$ are 3-bit sequences and $a_0, \cdots, a_6$ are 1-bit sequences. The 3-bit sequences $i_0, \cdots, i_2$ are input symbols of the (7,3)RS encoder and the RS encoder calculates its parity symbols using the input symbols. The primitive polynomial, $p(x)$, and the generator polynomial, $g(x)$, are

$$p(x) = x^3 + x + 1 \tag{3.4}$$

$$g(x) = (x-\alpha)(x-\alpha^2)(x-\alpha^3)(x-\alpha^4) \quad , \tag{3.5}$$

where α denotes a root of $p(x)$ [51]-[52]. The encoded 7 RS code symbols are input into the bi-orthogonal modulators and each input symbol selects the spreading code, c_j ($j = 0,\ldots,6$). Figure 2(b) shows a bi-orthogonal modulator structure. In this figure, the input symbol $b_j = (b_{j,0}, b_{j,1}, b_{j,2})$ is put into the code-selection module and one of the 8 Hadamard codewords is selected according to the bit combination of b_j, e.g., (0,0,1), and the selected codeword is outputted as c_j, e.g., (+1,-1,+1,-1,+1,-1,+1,-1). On the other hand, each of the seven 1-bit signals, $a_0, \cdots, a_6$, in Fig. 3.2(a) is modulated by BPSK and then spread by the spreading code, c_j. The spread sequence $s_0,\ldots,s_6$ is fed into the 8-point IFFT module. In this case, it is assumed that 1-point padding is applied to the IFFT. After the IFFT process, the output signal, $X(t)$, expressed in eq.(3.3), is parallel-to-serial converted and is preceded by a Guard Interval (GI).

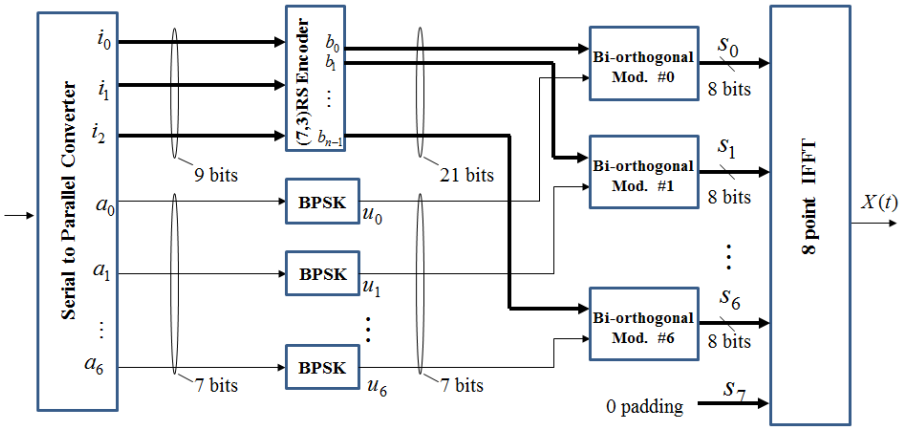

(a)

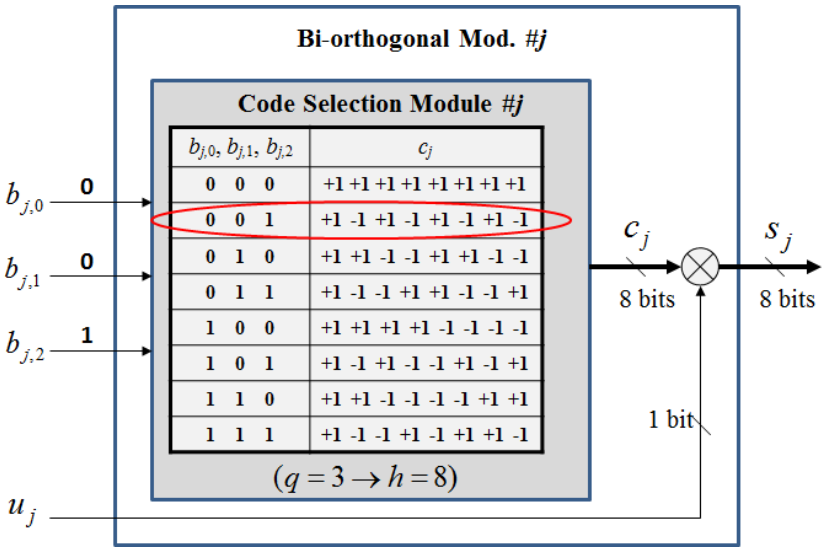

(b)

Fig. 3.2 (a) Example of the proposed transmitter
(b) Example of a bi-orthogonal modulator

3.2.2 Receiver Structure

Figure 3.3(a) shows the receiver structure of the proposed scheme. After removing GI, the received signal is serial-to-parallel converted and fed into the FFT. Then, the FFT output signals $\hat{s}_0,\ldots,\hat{s}_{n-1}$ are input into correlator banks, where correlation detection is performed.. Figure 3.3(b) shows the structure of one of the correlator banks. In this figure, one of the FFT output signals, $\hat{s}_j$, is input into h correlators in parallel and the correlator outputs $\lambda_0,\ldots,\lambda_{h-1}$ can be obtained. From these correlator outputs, the absolute values for them and their corresponding sign bit values (+1 or -1) are calculated. These absolute values are compared with each other and the maximum value $|\lambda_{\max}|$ is selected. The decision module estimates the transmitted code selection bits, $\hat{b}_j$, by performing the reverse procedure on the corresponding code-selection module in the transmitter and a code selection bits $\hat{b}_j$ is estimated. The same process is followed in all correlator banks. The estimated code-selection bits, $\hat{b}_0,\ldots,\hat{b}_{n-1}$, are fed to the RS decoder. In the RS decoder, a decoding procedure is performed and a decoded codeword is obtained. This decoded result is passed into the parallel-to-serial converter and fed back to the correlator banks. In the correlator banks, a decision procedure is performed using the fed-back RS codeword, $(\hat{i}_0,\ldots,\hat{i}_{n-1})$. In the decision module in Fig. 3.3(b), $\hat{a}_j$ is selected according to the value corresponding to the $\hat{i}_j$. After this procedure, the sign bits, $\hat{a}_0,\ldots,\hat{a}_{n-1}$, are determined and fed into the parallel-to-serial converter.

Figure 3.4 (a) is the receiver structure of an example case. This example has the same parameters as in Fig. 3.2 (a). In Fig. 3.4(b), a demodulation procedure for correlator bank #6 is illustrated. In this figure, each correlator calculates the correlator value using each assigned local correlation code, Cd_j ($j=0,\ldots,6$), and its sign bit value. Among the calculation results, the maximum absolute correlator value, $|\lambda_{\max}|$, is detected and its corresponding Hadamard codeword candidate, Cd_6, is selected. Then, the code-selection bits $\hat{b}_6$ are estimated as (1,1,0). The code-selection bits, $\hat{b}_6=(1,1,0)$ are fed into the RS decoder. The RS decoder corrects errors and provides a decoded codeword, $\hat{i}=(\hat{i}_0,\ldots,\hat{i}_6)$. An RS code symbol for the decoded codeword $\hat{i}_6=(0,0,1)$ is given back to correlator bank #6. At the Correlator bank #6, since $\hat{i}_6=(0,0,1)$ is not equal to $\hat{b}_6=(1,1,0)$, $\hat{i}_6=(0,0,1)$ is selected as the correct code-selection bits and its associated sign bit $\hat{a}_6=+1$ is provided. If $\hat{b}_6=(1,1,0)$ was not erroneous, $\hat{i}_6$ equals to $\hat{b}_6$ and the selected sign bit $\hat{a}_6=-1$ is provided.

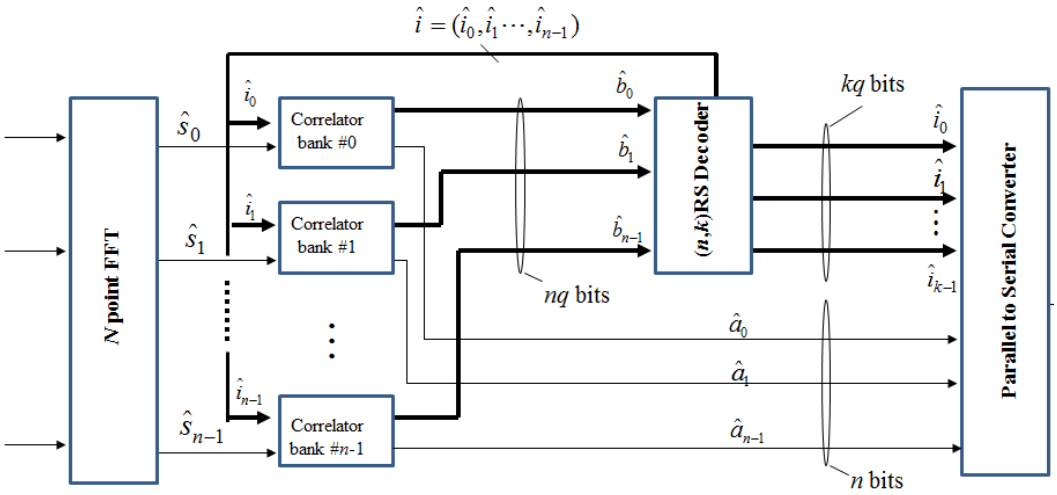

(a)

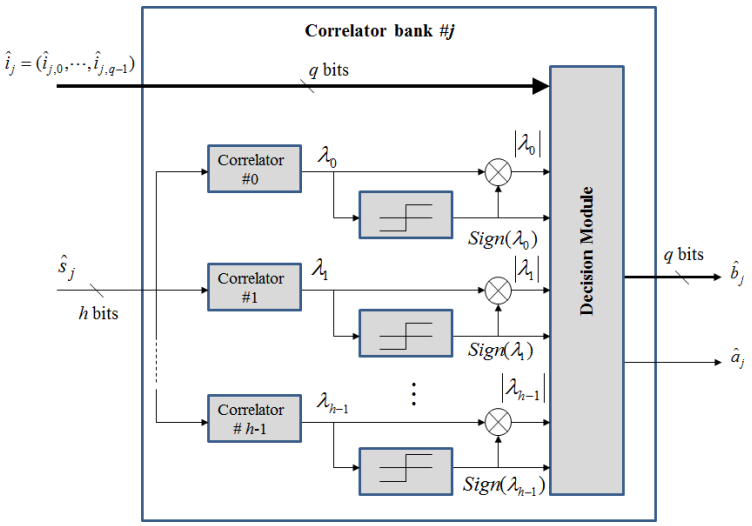

(b)

Fig. 3.3 (a) Receiver structure of the proposed scheme
(b) Correlator bank of the receiver

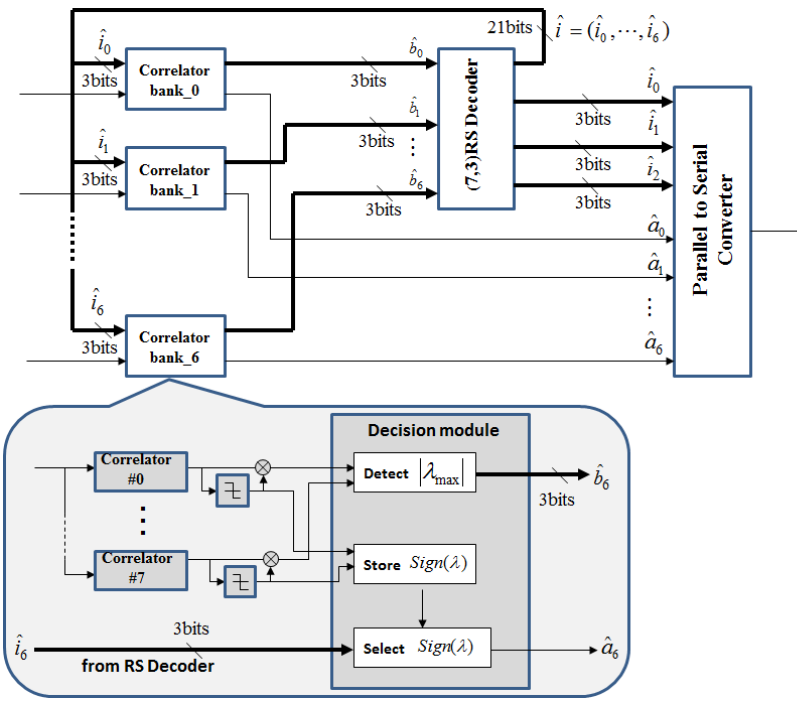

(a)

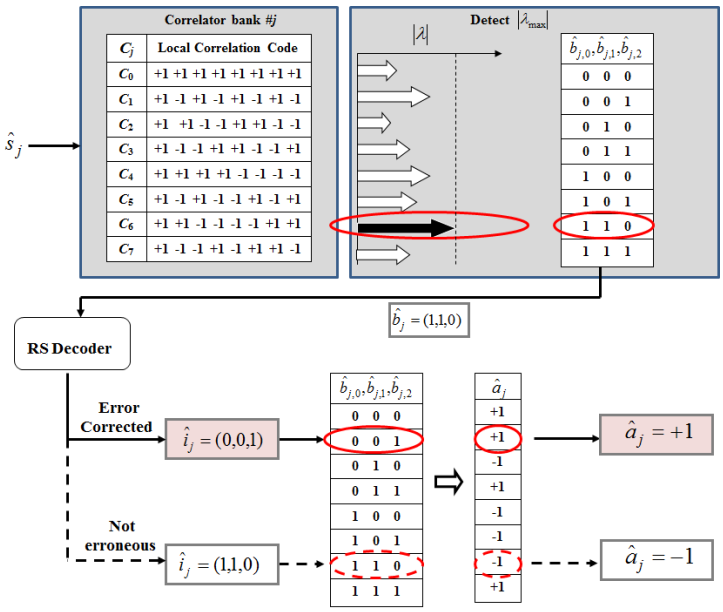

(b)

Fig. 3.4 (a) Example of the proposed receiver
(b) Example of the decoding Procedure

3.3. Performance Analysis

The code-selection error rate and the BER can be derived as follows. For the performance on an AWGN channel, without loss of generality, we only need to consider the performance when s_0 is transmitted. Let P_c denote the probability that the correlator bank #0 selects the correct correlator output and the sign bit is correctly detected.

In Fig. 3.3(b), the input signal of the correlator bank #0, $\hat{s}_0(t)$, is expressed as

$$\hat{s}_0(t) = s_0(t) + n_z(t)\,, \tag{3.6}$$

where $n_z(t)$ denotes an AWGN with a power spectral density of $\sigma^2 (= N_0 / 2)$.

From eq. (3.6), a correlator output of λ_m $(1 \le m \le h-1)$ can be derived as

$$\begin{aligned} \lambda_m &= \int_0^T \hat{s}_0(t) s_m(t) dt \\ &= \int_0^T s_0(t) s_m(t) dt + \int_0^T n_z(t) s_m(t) dt \end{aligned} \tag{3.7}$$

where $s_m(t)$ is a locally generated signal at the correlator #*m*.

The probability that the codeword that was sent will be chosen correctly is equal to the probability that the output of all of the other correlators will be smaller than that of the given correlator. Then P_c can be calculated as follows [64]-[66]:

$$\begin{aligned} P_c &= P_{rob}[\lambda_0 > 0, |\lambda_0| > (|\lambda_1|, \ldots, |\lambda_{h-1}|) \;\; |s_0] \\ &= \int_0^\infty p(\lambda_0) d\lambda_0 \prod_{m=1}^{h-1} P(|\lambda_m| < |\lambda_0|) \end{aligned} \tag{3.8}$$

where $p(\lambda_0)$ is the probability density function of the output of the correct correlator (correlator #0), and

$$P\left(\left|\lambda_m\right| < \left|\lambda_0\right|\right) = \int_{-\lambda_0}^{\lambda_0} p(\lambda_m) d\lambda_m \tag{3.9}$$

is the probability that the absolute value of the *m*-th incorrect correlator will be less than that of the correct correlator output. The second equality of eq. (3.8) holds because the correlator noise outputs are mutually independent.

Since the $p(\lambda_0)$ and $p(\lambda_m)$ are Gaussian probability distribution functions eq.(3.8) can be expressed as follows:

$$P_c = \int_0^{\infty} \frac{1}{\sqrt{2\pi\sigma^2}} \exp\left\{\frac{-(\lambda_0 - \sqrt{E_s})^2}{2\sigma^2}\right\} d\lambda_0 \left[\int_{-\lambda_0}^{\lambda_0} \frac{1}{\sqrt{2\pi\sigma^2}} \exp\left(\frac{-\lambda_m^2}{2\sigma^2}\right) d\lambda_m\right]^{h-1}. \tag{3.10}$$

Making the substitution $v = \left(\lambda_0 - \sqrt{E_s}\right)/\sigma$, $z = \lambda_m / \sigma$, P_c can be re-written as

$$\begin{aligned} P_c &= \int_{-\sqrt{2E_s/N_0}}^{\infty} \frac{1}{\sqrt{2\pi}} \exp\left(-\frac{v^2}{2}\right) \left[\int_{-\sqrt{2E_s/N_0}-v}^{\sqrt{2E_s/N_0}+v} \frac{1}{\sqrt{2\pi}} \exp\left(-\frac{z^2}{2}\right) dz\right]^{h-1} dv \\ &= \int_{-\sqrt{2E_s/N_0}}^{\infty} \frac{1}{\sqrt{2\pi}} \exp\left(-\frac{v^2}{2}\right) \left[1 - erfc\left(\frac{v + \sqrt{2E_s/N_0}}{\sqrt{2}}\right)\right]^{h-1} dv \end{aligned} \tag{3.11}$$

where. E_s denotes the symbol energy that can be expressed by bit energy E_b as follows [55]:

$$E_s = (q+1)E_b / r. \tag{3.12}$$

Then, the probability that a codeword is in error, P_E, is derived as

$$P_E = 1 - P_c. \tag{3.13}$$

From eq. (3.11), the probability that the selection code is correctly detected but its sign bit is not correct, P_{sg_c}, can be calculated as.

$$\begin{aligned} P_{sg\_c} &= P_{rob}[\lambda_0 < 0, |\lambda_0| > (|\lambda_1|,\ldots,|\lambda_{h-1}|) \ |s_0] \\ &= \int_{-\infty}^{-\sqrt{2E_s/N_0}} \frac{1}{\sqrt{2\pi}} \exp\left(-\frac{v^2}{2}\right)\left[-1+erfc\left(\frac{v+\sqrt{2E_s/N_0}}{\sqrt{2}}\right)\right]^{h-1} dv. \end{aligned} \tag{3.14}$$

From eqs.(3.13) and (3.14), the probability that the Hadamard code is wrongly selected among the $h-1$ candidates is given by

$$P_{cs} = P_E - P_{sg\_c}\,. \tag{3.15}$$

The code-selection error after the RS decoding, P_{cs_RS} is regarded as the symbol error of the RS code. Since the symbol error before the RS decoder can be given by P_{cs} , P_{cs_RS} can be approximately expressed as

$$P_{cs\_RS} = \frac{1}{n}\sum_{j=t+1}^{n}\binom{n}{j} P_{cs}{}^{j}(1-P_{cs})^{n-j}\,, \tag{3.16}$$

where t denotes the correction ability of an (n,k) RS code [55]-[56].

Using Bayes' theorem, BER for P_{cs_RS} is derived as below:

$$P_{b\_cs\_RS} = \frac{2^{q-1}}{2^q-1} P_{cs\_RS}\,. \tag{3.17}$$

Next, we derive the probability of the sign bit errors. The sign bit error occurs in either of the following case: (a) λ_0 is detected correctly but its sign is incorrect, (b) λ_0 is not detected correctly and its sign is also incorrect. The probability of the case (a) is given by eq.(3.14). The probability of the case (b) is derived as follows. In the $(q+1)$-bit bi-orthogonal modulator input bits, the total number of combinations in which u bits are erroneous is $\sum_{u=1}^{q+1}\binom{q+1}{u} = 2^{q+1}-1$. Among the $2^{q+1}-1$ combinations, the total number of cases where the sign bit and the u bits out of q bits are

erroneous is $\sum_{u=1}^{q}\binom{q}{u} = 2^q - 1$.

From the above, the probability of the case (b) can be calculated as $\frac{2^q - 1}{2^{q+1} - 1} P_{cs}$.

Then, the probability of the sign bit errors P_{sgn_ber} can be expressed as

$$P_{\text{sgn}\_ber} = \frac{2^q - 1}{2^{q+1} - 1} P_{cs} + P_{sg\_c} \quad . \tag{3.18}$$

Eq.(3.18) expresses the sign BER before the RS decoding codeword is provided to the correlator bank. After this takes place and re-correlation detection is performed, the sign BER, $P_{\text{sgn}\_ber\_fb}$, can be given by

$$P_{\text{sgn}\_ber\_fb} = \frac{2^q - 1}{2^{q+1} - 1} P_{cs\_RS} + P_{sg\_c} \quad . \tag{3.19}$$

We can calculate the total BER that includes both the BER of the sign bit and the BER caused by erroneous code selection as follows:

$$P_{totalBER\_RS} = \frac{1}{q+1}(q \cdot P_{b\_cs\_RS} + P_{\text{sgn}\_ber\_fb}) \, . \tag{3.20}$$

Table 3.1 Simulation parameter on an AWGN channel

	q	n	k	$h = 2^q$	$N = 2^q$	r
(7,5)RS code	3	7	3	8	8	0.786
(15,11)RS code	4	15	11	16	16	0.787
(63,47)RS code	6	63	47	64	64	0.782

3.4. Numerical Results

3.4.1 Performance on an AWGN Channel

The numerical performance results of the proposed scheme are presented. Figure 3.5 shows the performance of the code-selection error rate. The proposed scheme is compared with the uncoded scheme. The evaluation parameters are listed in Table 3.1. The coding rate of the RS code r is chosen so as to be around 0.78. In Fig.3.5, we can see that the proposed scheme improves the code-selection error rate compared with the uncoded scheme. At the level of 10^{-5}, the coding gains for the (7,5)RS code, (15,11)RS code and (63,47)RS code are approximately 1.2 dB, 1.8 dB and 3.0 dB, respectively. Moreover, a higher coding gain can be achieved as the RS codeword becomes longer.

Figure 3.6 shows the improvement in the sign BER when employing the RS decoding feedback. In Fig.3.6, the figure clearly indicates that we can obtain significant improvements. As stated in the previous section, the sign bit error occurs in either of the following cases: (a) code selection is correctly detected but its sign is incorrect, (b) code selection is not detected correctly and its sign is also incorrect. From eq. (3.14), it is found that the sign BER caused by (a) is potentially very low. Therefore, from eq. (3.19), improving the probability of case (b) by RS decoding feedback reduces the sign BER remarkably. At the level of 10^{-5}, the coding gains of 2.3 dB, 3.0 dB and 3.8 dB are obtained for the (7,5)RS code, (15,11)RS code and (63,47)RS code, respectively. Note that RS decoding feedback is an efficient method in that both code-selection error and sign bit error can be corrected by a single error correction code. The total BER of the proposed scheme, which is the total probability of the bit errors for the code-selection module and the sign bit, is shown in Fig. 3.7. In this figure, it is observed that the proposed scheme achieves remarkable coding gains. In the level of BER $=10^{-5}$, it is shown that the proposed scheme attains the coding gains by 1.2 dB, 1.8 dB and 3.0 dB when the (7,5)RS code, (15,11)RS code and (63,47)RS code, respectively, are applied.

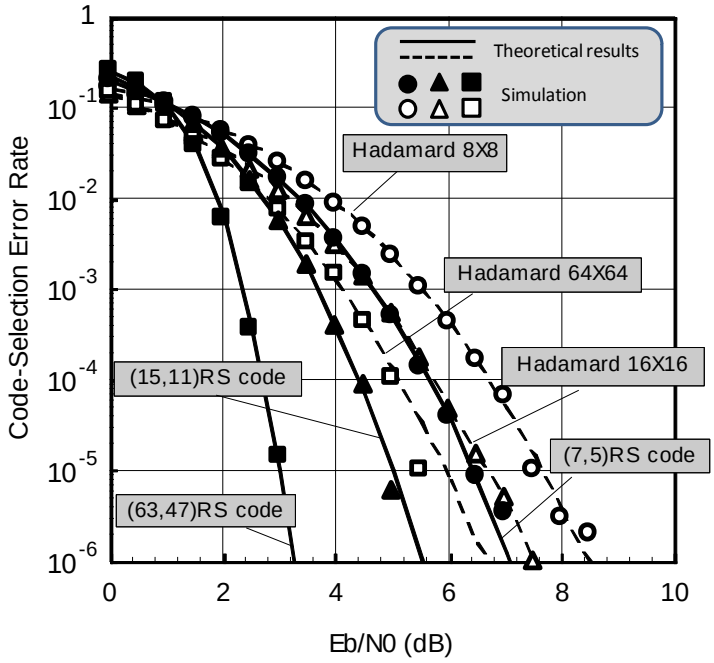

Fig. 3.5 Code-selection error rate on an AWGN channel

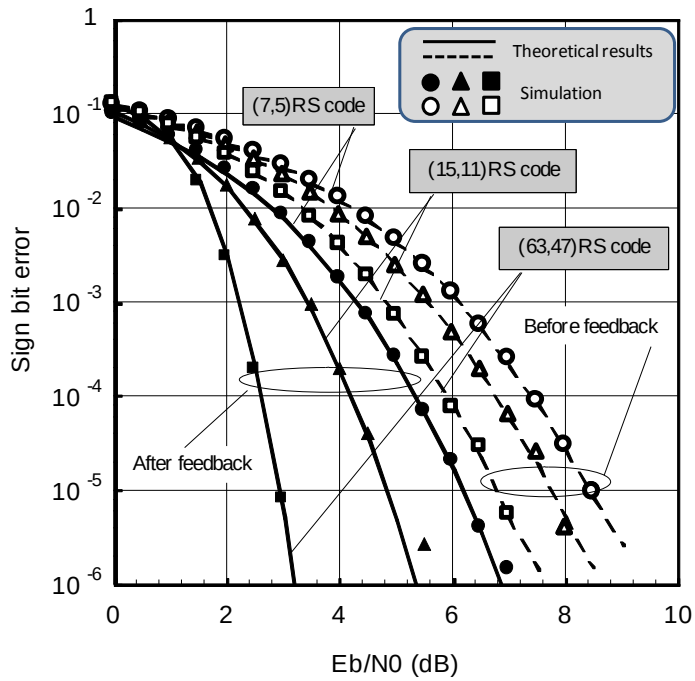

Fig. 3.6 Sign bit error rate on an AWGN channel

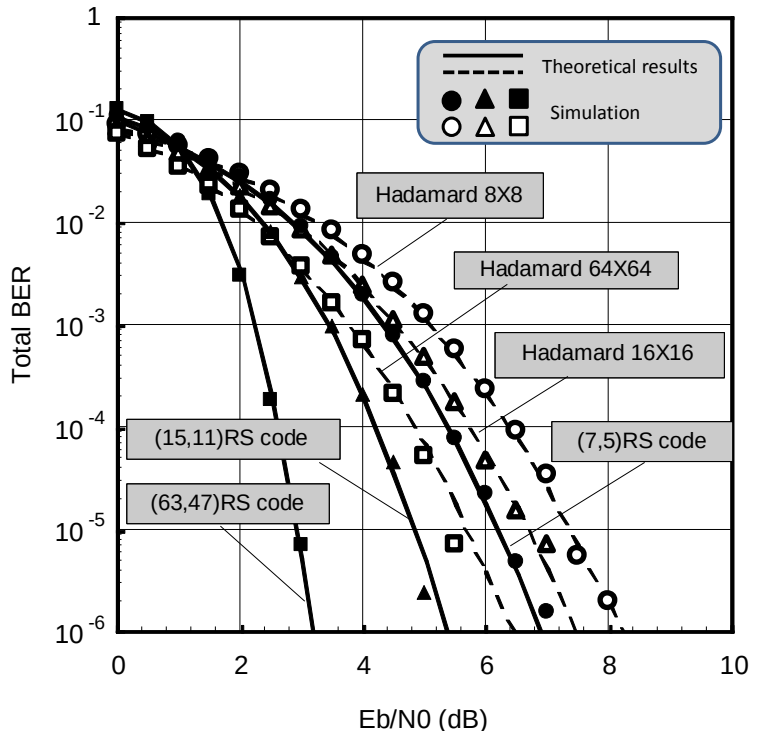

Fig. 3.7 Total BER performance on an AWGN channel

Table 3.2 Simulation parameters on fading channels

Modulation	BPSK
Coding	(63,55), (63,47), (63,33), (15,7) RS code r_c=1/2, K=7 conv. code (for comparison)
Hadamard code	h=64
Number of FFT (Number of subcarriers)	N=64
Fading Model	two-path Rayleigh fading DUR=0.0dB f_DT=2.0×10^{-5}, 1.56×10^{-4}, 2.5×10^{-3}
Delay Spacing	τ_d/T_s =1.56×10^{-2}, 7.8×10^{-2} , 1.40×10^{-1} (τ_d :path delay, T_s :OFDM symbol duration)
Guard Interval	T_g=0.16T_s
Interleave	Inter-subcarrier interleaving

3.4.2 Performance on Multi-path Fading Channels

The simulation results for the proposed scheme on multi-path fading channels are presented. A multi-path fading model is assumed to be a two-path Rayleigh fading model with DUR = 0.0 dB, which gives one of the severest channel conditions. Table 3.2 shows the simulation parameters. In Table 3.2, it is assumed that the path delay spread, τ_d , does not exceed the GI length.

The code-selection error rate is shown in Fig. 3.8. it can be seen that the overall higher error correction ability codes have better performance. The performance of the (63,33)RS code and the (63,47)RS code on the fading with $f_DT = 2.5\times10^{-3}$ offer remarkable improvements. On the fading with $f_DT = 2.0\times10^{-5}$, the performances of the three codes have marginal differences. The above performance difference due to f_DT comes from the length of the burst errors. The code selection error rates for the proposed scheme employing the (63,47)RS code with different delay spacings, τ_d / T_s, are plotted in Fig. 3.9. The selected τ_d / T_s values are shorter than the length of GI.

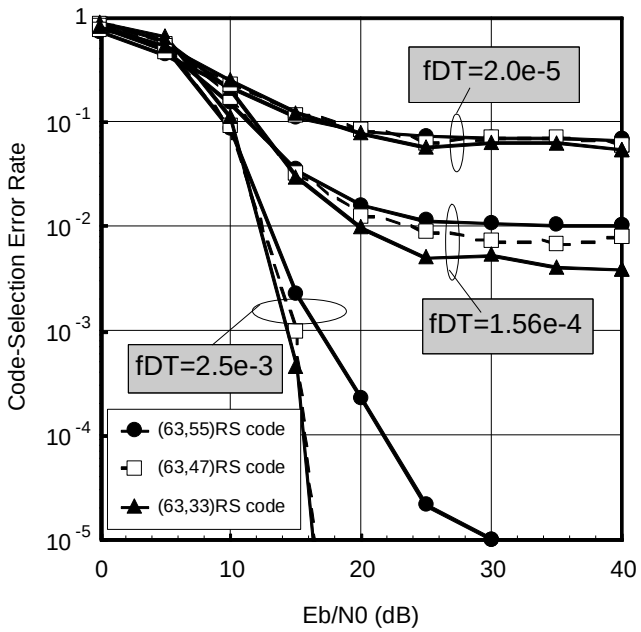

Fig. 3.8 Code-selection error rate of the proposed scheme on fading channels

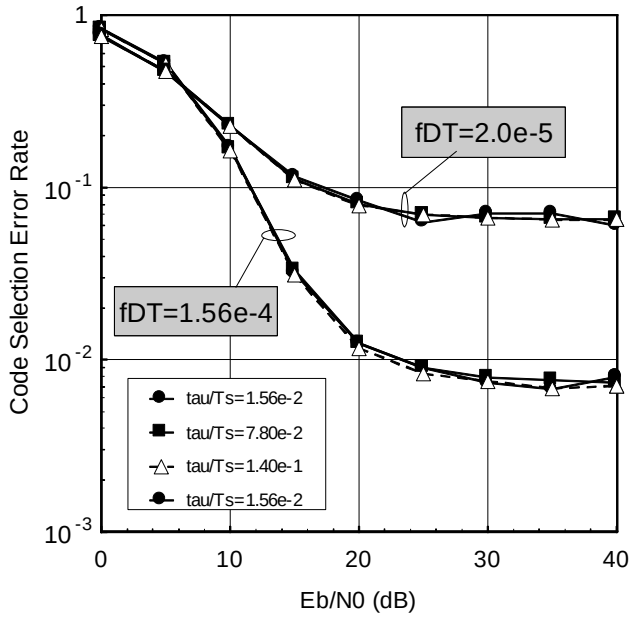

Fig. 3.9 Code-selection error rate of the proposed scheme employing (63,47)RS code on fading channels

It is found that the performance differences of the curves on both fading channels are marginal. One might expect that the distribution of the erroneous symbols in an RS codeword is different, but approximately the same number of symbol errors occur due to the difference of τ_d / T_s.

Figure 3.10 shows a comparison between the RS code and the convolutional code. As an example case for convolutional codes, a code with widely used rate, $r_c = 1/2$, and constraint length, $K = 7$ is evaluated [48]-[49],[56]. Generally, it is not easy to compare the performances of the block code and the convolutional code under equivalent conditions. Therefore, two kinds of parameters, coding rate and minimum distance, are chosen to be aligned. Since the coding rate and the minimum distance of the convolutional code are 1/2 and 10, respectively, the corresponding RS codes are chosen to be the (63,33)RS code and (63,55)RS code, respectively. Note that the (63,55)RS code can obtain a higher throughput (transmission in bits per second per Hz) than the convolutional code, because the coding rate of the (63,55)RS code is higher than that of the convolutional code. To compare the performances of the both codes under equivalent conditions, both the RS code and the convolutional code use the same transmitter and receiver structures. The only difference is that the encoder and decoder of the RS code are replaced with those of the convolutional code. In the convolutional code case, the code-selection bits for all subcarriers are convolutionally encoded by a single encoder.

The Viterbi decoder output (corresponding to $(\hat{i}_0,\ldots,\hat{i}_{n-1})$ in Fig. 3.3 (a)) is fed back into the correlator banks. In Fig.3.10, it is shown that the curve of the (63,33)RS code has a better performance than that of the convolutional code over the three fading channels. It can be said that the burst error correction ability of the RS code works effectively works on the fading channels. This correction ability is higher than that of the convolutional code because the convolutional code is a bit error correction code. The lower the code-selection error rates, the lower the total BER performances. Compared with the convolutional code and the (63,55)RS code, the BER performance of the RS code is slightly better than that of the convolutional code. On the channel of $f_D T = 1.56\times10^{-4}$, the performance difference is marginal in the region of high Eb/N0. In this evaluation, the convolutional code and the interleaving are applied in the frequency domain. This coding method is beneficial in that a single encoder/decoder structure can easily be formed over the all subcarriers. On the other hand, there are many cases in which the convolutional code and the interleaving are applied in the time domain. In this method, better performances of the convolutional code may be expected. However, from the viewpoint of implementation complexity, it is required that the number of

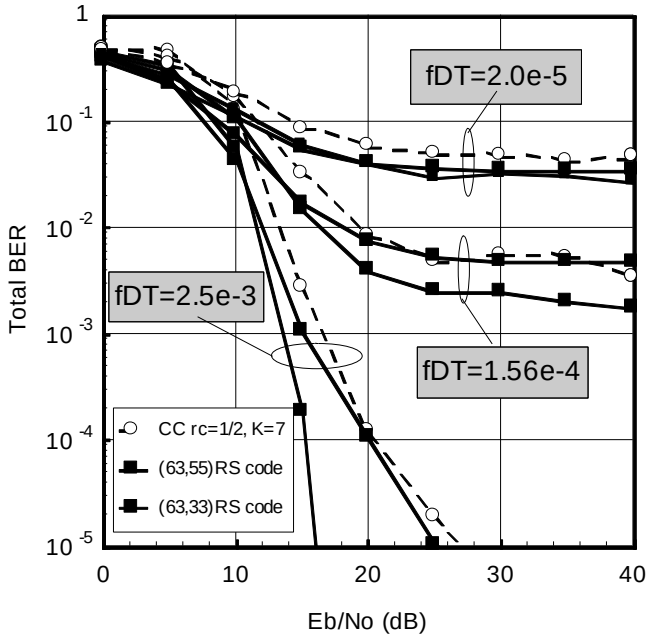

Fig. 3.10 Comparisons of the total BER performance of the proposed scheme and convolutional coding scheme on fading channels

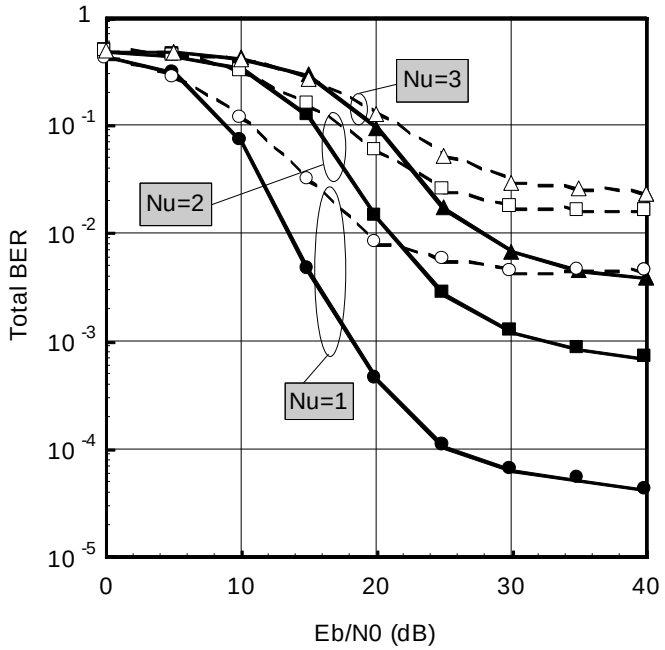

Fig. 3.11 Total BER performances of the proposed scheme on fading channels

encoders/decoders be the same as that of the subcarriers, or that the encoder/decoder processing be higher. Figure 3.11 shows the multiple access performances on the channels of $f_D T = 2.0 \times 10^{-3}$ and $f_D T = 1.56 \times 10^{-4}$ channels. Each transmit employs a (15,7) RS code, and the system parameters are set as follows: $q = 4$, $h = 2^q = 64$, $n = 2^q - 1 = 15$, $k = 7$ and $N = 2^q = 64$. In this case, 16 codewords among the 64 Hadamard codewords are assigned to each transmitter and the maximally accessible users, $N_{\max}$, are 4. For simplicity, it is assumed that the users transmit signals synchronously. In Fig. 3.11, the total BER performances are plotted when N_u users are active. The curves on $f_D T = 2.0 \times 10^{-3}$ channel appear to be relatively better than those on $f_D T = 1.56 \times 10^{-4}$ channel and this trend is the same as those in Figs. 3.8 and 3.10. It is also found that the performances are degraded on both fading channels as N_u increases and that the degradation level on $f_D T = 2.0 \times 10^{-3}$ is larger than that on $f_D T = 1.56 \times 10^{-4}$.

3.5 Conclusion

In this chapter, we proposed an error correction scheme that is suitable for an MC-DS-CDMA system with bi-orthogonal modulation. To employ an efficient error coding, an RS code for code-selection bits and no error correction code for sign bits were proposed. The code-selection error and BER performance on an AWGN channel were evaluated by theoretical analysis and simulations, and the performances on multi-path fading channels were also evaluated. It was shown that the proposed scheme obtained remarkable improvements over uncoded schemes. The performance comparisons with convolutional coding schemes on multi-path fading channels clarified that the proposed scheme could obtain higher improvements. The multiple access performances on the fading channels showed that the performances degraded as the number of users increased.

In this chapter, as basic performance evaluations of the proposed scheme, BPSK was employed for the sign bit-modulation scheme. However, in order to achieve higher frequency utilization efficiency, the application of a multi-level modulation should be further considered. As for the error correction codes, the RS code was found to be a simple and suitable code for this system.

Chapter 4

Adaptive Trellis Coded Modulation Applied to MC-DS-CDMA

4.1. Introduction

A GSRI ATCM is applied to a MC-DS-CDMA system with bi-orthogonal keying is analyzed. The MC-DS-CDMA being considered is one in which the input sequence of a bi-orthogonal modulator has a code-selection bit sequence and sign bit sequence. In Chapter 3, an efficient error correction code using the RS code for its code-selection bit sequence has been proposed. However, since BPSK is employed for the sign-bit modulation, no error correction code is applied to it. To realize a high-speed wireless system, a multi-level modulation scheme (e.g., MPSK and MQAM) is desired.

In this chapter, we investigate the performance of the MC-DS-CDMA with bi-orthogonal keying employing GSRI ATCM. GSRI TC-MPSK can arbitrarily set the bandwidth-expansion ratio to maintain higher coding gain than the conventional pragmatic TCM scheme. By changing the modulation scheme and the bandwidth-expansion ratio (coding rate), this scheme can optimize the performance according to the channel conditions. The performance evaluations by simulations on an AWGN channel and multi-path fading channels are presented.

Additionally, in Section 4.5, the performance of the MC-DS-CDMA with GSRI ATCM employing practical SNR estimation is presented. The selection of the modulation and coding

scheme for ATCM is assumed to be an ideal method described in [61]. However, since the modulation and coding selection is based on the ideal SNR estimation method, the adaptation thresholds are designed according to the BER performance on an AWGN channel [61] and performance evaluations employing practical channel estimation schemes are desired. In this section, an application of a practical SNR estimation method to the ATCM scheme is considered.

Finally, in Section 4.6, the performance of a simplified scheme in terms of complexity reduction is investigated. The system structure of the transmitter requires multiple numbers of GSRI-ATCM encoders and decoders. This implies that the system complexity increases along with an increase in the number of subcarriers. The performance of the GSRI ATCM MC-DS-CDMA when the numbers of encoders and decoders are reduced (hereinafter called a simplified scheme). In reducing the number of encoders and decoders, the method of selecting the coding rate and modulation index is modified.

4.2 System Description

4.2.1 Transmitter Structure

The transmitter structure of the proposed scheme is given in Fig. 4.1. The incoming binary bits are serial-to-parallel converted into $kq+\sum m_j$ parallel bit streams, where k is the number of the input sequences to the RS encoder and q is the number of bits in each input sequence. These k input sequences, $i=(i_0,\ldots,i_{k-1})$, are fed into the (n,k)RS encoder over GF(2^q). The encoded symbols, $b_0,\ldots,b_{n-1}$, are inputted into n code-selection modules and each module selects an orthogonal code. In the code-selection module, the orthogonal code used here is Hadamard code. When the q bits b_j ($j=0,\ldots,n-1$) are fed into the modulator, one of the h Hadamard codewords is selected according to the bit combination of b_j and the selected codeword is outputted as c_j. In this section, $h=2^q$ $(=n+1)$ is assumed. On the other hand, n parallel sign bit signals $u_0,\ldots,u_{n-1}$ are encoded and modulated by GSRI-TCM modules (the detailed function is explained later) and $a_0,\ldots,a_{n-1}$ are spread by the selected Hadamard codewords $c_0\cdots c_{n-1}$, respectively. The modulated sequences $s_0,\ldots,s_{n-1}$ are fed into the inter sub-carrier interleaver and they are randomized due to the random interleaver. The number of the interleaver input signals are the same as in the N- point IFFT.

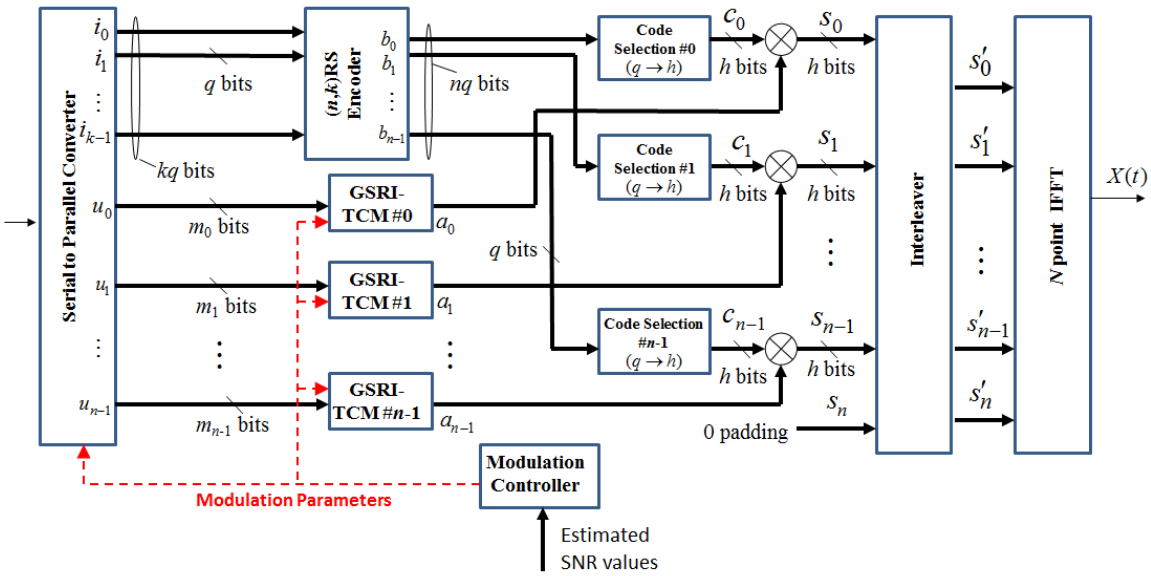

Fig. 4.1 Transmitter structure

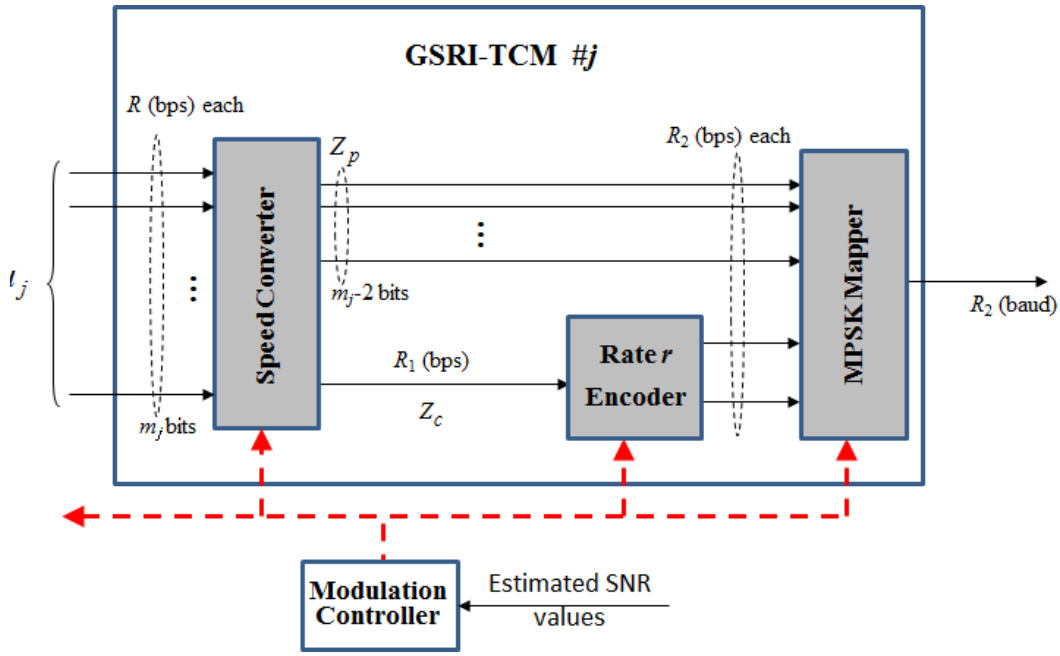

Fig. 4.2 GSRI Pragmatic TC-MPSK encoder structure

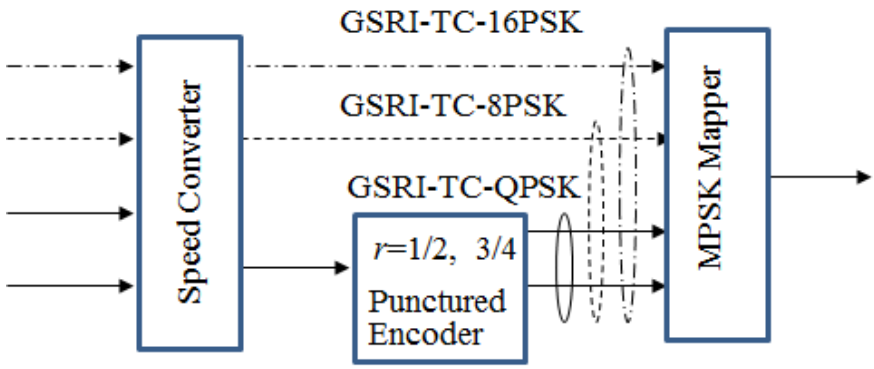

Fig. 4.3 Example of GSRI Pragmatic TC-MPSK

Table 4.1 Examples of combinations of m_j, r and R_2/R

$m_j - 2$	r (%)						
	7/8	6/7	5/6	4/5	3/4	2/3	1/2
0	114.3	116.7	120.0	125.0	133.3	150.0	200.0
1	109.1	110.5	112.5	115.4	120.0	116.7	150.0
2	106.7	107.7	109.1	111.1	114.3	120.0	133.3

4.2.2 GSRI Trellis Encoder

To explain the GSRI trellis encoder more precisely, the general structure of the GSRI Pragmatic TCM encoder is shown in Fig.4.2. The m_j-bit ($m_j \geq 2$) parallel sequence, u_j, is input into the speed converter where the signals are converted at the rate of. R bit/sec into two kinds of signals: one is 1 bit sequence, Z_c with R_1 bits/s and the other is an $m_j - 2$ bit sequence, Z_p with R_2 bits/s.

The $m_j - 2$ bit signals are directly inputted to the mapper, while 1 bit signal is input to the rate r -convolutional encoder and the encoder outputs 2 bit signals to the mapper. The rate, r, is arbitrarily set using a punctured code based on the best-known rate 1/2 convolutional code. The mapper assigns m_j bit signals to one of the 2^{m_j} points, which are selected based on double-Gray-coded mapping [59]. The two least significant bits corresponding to the outputs of the convolutional encoder select one of the four signals based on the Gray-coded scheme. Using the other $m_j - 2$ bits, a sector in the signal space is also selected according to the Gray-coded scheme. This mapping can be expected to improve the error performance occurring in neighboring sectors. All the mapper input signals, both the $m_j - 2$ uncoded bits and the 2 coded bits, must be at R_2 bits/s, respectively.

The bandwidth expansion ratio R_2/R is expressed as follows [59]:

$$\frac{R_2}{R} = \frac{m_j}{2r + m_j - 2} \quad . \tag{4.1}$$

In eq. (4.1), it is found that R_2/R is derived from m_j and r. This implies that the bandwidth-expansion ratio can be arbitrarily set when a modulation scheme is chosen. It is expected

that this scheme achieves higher coding gain as the bandwidth-expansion ratio increases. On the other hand, the conventional Pragmatic TCM fixes the r uniquely, once the modulation scheme is determined.

For example, Fig.4.3 shows the construction of the GSRI Pragmatic TCM in the case of r = 3/4. In Fig.4.3, the modulation schemes of QPSK, 8PSK and 16PSK correspond to the number of input signal bits, m_j, being 2, 3 and 4, respectively. The bandwidth expansion ratios (R_2/R) for the QPSK, 8PSK, and 16PSK cases are 4/3 (133.3 %), 6/5 (120 %) and 8/7 (114.3 %), respectively. Table 4.1 lists examples of combinations of r, m_j and R_2/R.

4.2.3 Receiver Structure

Figure 4.4 shows a receiver structure of the proposed scheme. After removing GI, received signal is serial-to-parallel converted and fed to FFT. Then FFT output signals are de-interleaved in the inter sub-carrier de-interleaver and the output signals $\hat{s}_0,\ldots,\hat{s}_{n-1}$ are inputted into correlator banks. In each correlator bank, correlation detection is done. In the correlator bank, one of the FFT output signals $\hat{s}_j$ is inputted to h correlators in parallel and the correlator outputs $\lambda_0,\ldots,\lambda_{h-1}$ can be obtained. From these correlator outputs, the absolute values of them are compared with each other and the maximum value $|\lambda_{\max}|$ is detected. The decision module estimates the transmitted code selection bits $\hat{b}_j$ by doing reverse procedure of the corresponding code selection module in the transmitter and a code selection bits $\hat{b}_j$ is estimated. The same process is done in all correlator banks. The $\hat{b}_0,\ldots,\hat{b}_{n-1}$ are fed to RS decoder. In the RS decoder, decoding procedure is performed and a decoded codeword is obtained. This decoded result is passed to the parallel-to-serial converter as well as fed back to the correlator banks. In the correlator banks, decision procedure is done using the fed back RS codeword $(\hat{i}_0,\ldots,\hat{i}_{n-1})$. In the decision module, $\hat{a}_j$ is selected according to the value corresponding to the $\hat{i}_j$. After this procedure, the sign bits $\hat{a}_0,\ldots,\hat{a}_{n-1}$ are determined and fed to the trellis decoder.

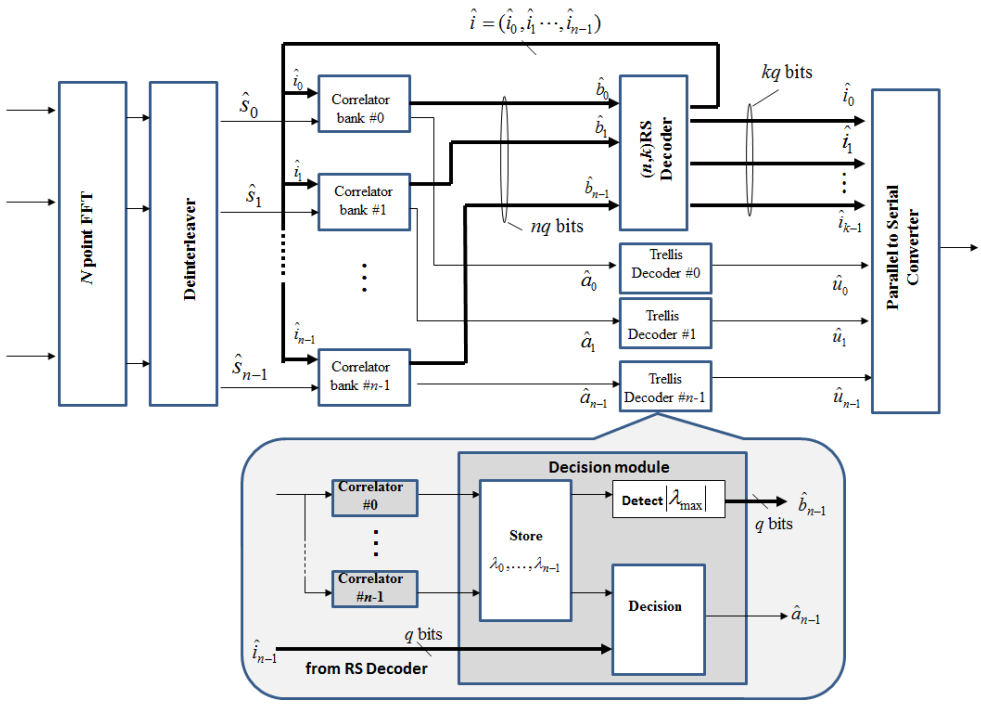

Fig. 4.4 Receiver structure

Table 4.2 Simulation parameter on an AWGN channel

	q	n	k	$h = 2^q$	$N = 2^q$
(63,47)RS code	6	63	47	64	64

4.3 Performance Evaluation on AWGN Channel

In this section, the BER of the proposed scheme on an AWGN channel is presented. As an example case the simulation parameters are listed in Table 4.2.

Figure 4.5 shows the performances of the sign bits. The sign bits are encoded and modulated by the GSRI Pragmatic TCM. In this figure, the conventional Pragmatic TCM can only set the convolutional coding rate of r = 1/2 and the selectable modulation scheme is fixed according to the number of parallel transitions. Therefore, the conventional pragmatic TCM has a total of three cases, r = 1/2 QPSK, r = 1/2 8PSK and r = 1/2 16PSK. On the other hand, the GSRI Pragmatic TCM can set the coding rate arbitrarily and both r = 1/2 and 3/4 can be selected in these figures. In Fig.4.5, the difference between r = 1/2 TC-8PSK and r = 3/4 TC-QPSK is marginal. However, we can see overall that the BER performance attained improves as the frequency utilization efficiency listed in Table 4.3 is reduced. This implies that, by increasing the coding rate and modulation scheme, more information can be transmitted. It is also said that the GSRI Pragmatic TCM can set more channel sensitive parameters compared with the conventional pragmatic TCM. This figure is used for deciding the adaptation thresholds that change the coding rate and modulation schemes. The thresholds are obtained using the set of BER performance curves of all the different codes on AWGN so that BER is kept below a certain *error roof* [61]. In this figure, examples of *error roofs* of 10^{-2} and 10^{-4}, and their corresponding adaptation thresholds (μ_1, μ_2, μ_3 and μ_4) are depicted. Figure 4.6 shows the total BER performances. In this figure, the curves of the BER indicate the combined BER of the sign BER for each GSRI Pragmatic TC-MPSK and the code-selection BER. Comparing with Fig. 4.5, the same trend of the performance can be seen. However, the curves of r=1/2 TC-QPSK, r = 3/4 TC-QPSK and r = 1/2 TC-8PSK have approximately the same performance.

Table 4.3 Frequency utilization efficiency

Modulation scheme	Rate of convolutional encoder (r)	Freq. Utilization Efficiency (bit/sec/Hz)
GSRI TC-QPSK	1/2	1.0
	3/4	1.5
GSRI TC-8PSK	1/2	2.0
	3/4	2.5
GSRI TC-16PSK	1/2	3.0
	3/4	3.5
Conv. TC-QPSK	1/2	1.0
Conv. TC-8PSK	1/2	2.0
Conv. TC-16PSK	1/2	3.0

Table 4.4 Simulation parameters on multi-path fading channels (AWGN based adaptation thresholds)

Sign bit Modulation	GSRI Pragmatic ATC-MPSK Conv. Pragmatic ATC-MPSK
RS Coding	(63,47)RS code
Hadamard code	h=64
Number of FFT (Number of sub-carriers)	N=64
Fading Model	two-path Rayleigh fading DUR=0.0dB f_DT= 1.56×10^{-4}, 1.25×10^{-5}
Delay Spacing	τ_d/T_s =1.56×10^{-2} (τ_d :path delay, T_s :OFDM symbol duration)
Guard Interval	T_g=0.16T_s
Channel Estimation	Perfect channel estimation
Adaptive Threshold	AWGN Based Thresholds

4.4 Performance Evaluation on Multipath Fading Channels

4.4.1 Evaluation Conditions

The performances of the adaptive coding and modulations on multi-path fading channels are evaluated. The simulation parameters are described in Table 4.4. We evaluate the performances on a two-path Rayleigh fading channel with DUR = 0.0 dB, which is one of the severest channel models. To evaluate the basic performances, the following assumptions are made.

- The channel estimation for each sub-carrier is perfectly known and this information is utilized in the modulation controller without delay.
- The receiver can detect the phase rotation of the received signal and is ideally compensated.
- The coding rate and modulation scheme are changed based on an instantaneous SNR [61] of the received pilot signal for each sub-carrier. These SNRs are precisely calculated at the modulation controller.

For simplicity, the SNR estimation is performed as follows. In Fig.4.1, the known signals modulated by BPSK, $a_0,...,a_{n-1}$, whose signal space has unit energy ($E_s = 1$) are transmitted and distorted by only fading. The output, $\hat{a}_0,...,\hat{a}_{n-1}$, of the receiver in Fig.4.4 can be obtained. In this case, the RS decoding feedback is not applied. Given the variance of Gaussian noise $\sigma^2 = N_0 / 2$, the instantaneous SNR at the ℓ-th sub-carrier is calculated as $\hat{a}_\ell{}^2 / \sigma^2$.

Table 4.5 shows the adaptation thresholds and their corresponding coding and modulation schemes. As stated in the previous section, the adaptation thresholds are chosen -using the performance curves of individual schemes on AWGN- to keep the BER below an *error roof* [61]. Figure 4.7 depicts this concept and is used for deciding the adaptation thresholds. When the *error roof* is set to BER = 10^{-2}, μ_1, μ_2, μ_3 and μ_4 are 2.0, 2.8, 4.8 and 8.0 dB, respectively. In the case where the *error roof* is BER=10^{-4}, μ_1, μ_2, μ_3 and μ_4 are 2.8, 5.0, 6.8 and 10.8 dB, respectively. As the error roof is lowered, the thresholds for all schemes move to the right. That is, schemes with better BER performances (and lower throughputs) are employed more often.

Table 4.5 Adaptation thresholds

Scheme	Adaptation threshold	Coding and Mod.
GSRI Pragmatic TC-MPSK	$SNR < \mu_1$	r=3/4 TC-QPSK
	$\mu_1 \le SNR < \mu_2$	r=1/2 TC-8PSK
	$\mu_2 \le SNR < \mu_3$	r=3/4 TC-8PSK
	$\mu_3 \le SNR < \mu_4$	r=1/2 TC-16PSK
	$\mu_4 \le SNR$	r=3/4 TC-16PSK
Conv. Pragmatic TC-MPSK	$SNR < \mu_1$	r=1/2 TC-QPSK
	$\mu_1 \le SNR < \mu_3$	r=1/2 TC-8PSK
	$\mu_3 \le SNR$	r=1/2 TC-16PSK

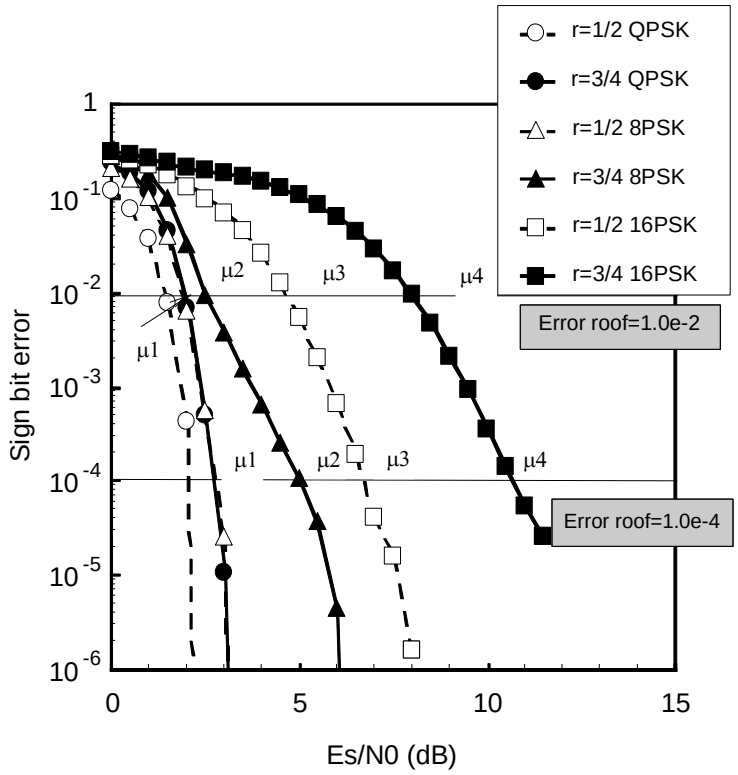

Fig. 4.5 Sign bit error rate on an AWGN channel ((63,47)RS coded MC-DS-CDMA)

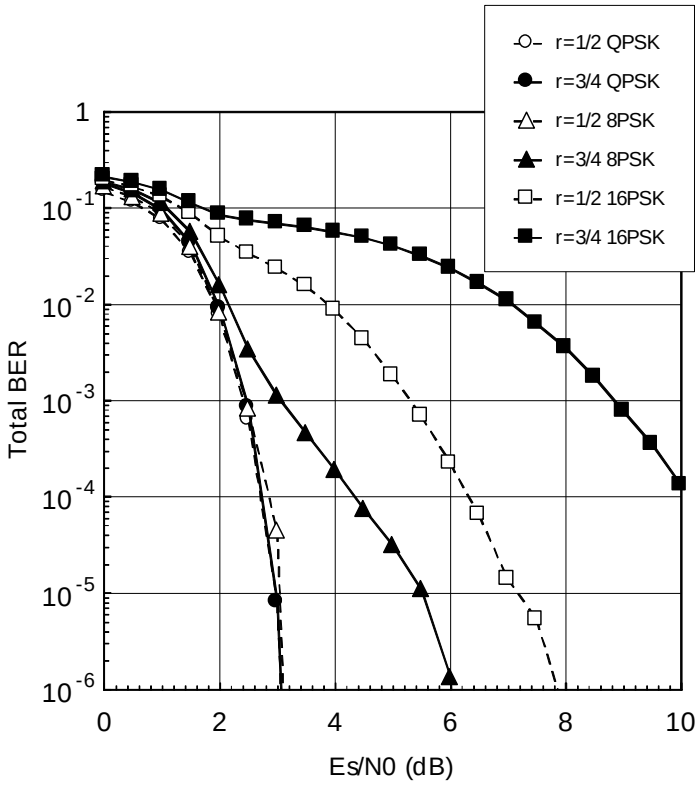

Fig. 4.6 Total BER performance on an AWGN channel ((63,47)RS coded MC-DS-CDMA)

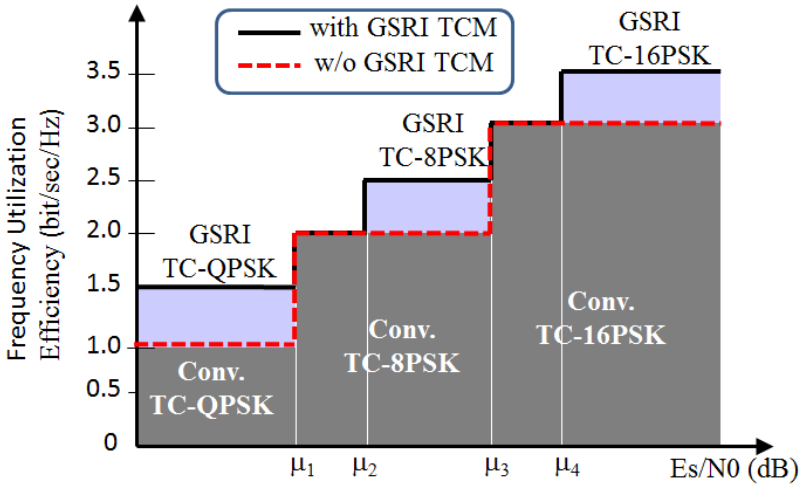

Fig. 4.7 Frequency utilization efficiency and adaptation thresholds

4.4.2 BER Performance

The total BER performances of the proposed and conventional Pragmatic TCM schemes on the multi-path fading of $f_D T = 1.56 \times 10^{-4}$ are shown in Fig. 4.8. In this figure, the *error roof* is set to BER = 10^{-2} and 10^{-4}. Comparing the performance of the proposed scheme with that of the conventional Pragmatic TCM scheme, it is shown that the BER performance is approximately the same in the region of low Es/N0. When Es/N0 is higher than 10 dB, the conventional Pragmatic TCM scheme has better performance than the proposed scheme. This is because that the conventional Pragmatic TCM scheme chooses only the coding rate of r = 1/2 case for every modulation scheme and this parameter selection keeps the BER lower than that of the proposed scheme. At the BER = 10^{-4} level, the difference of the coding gain between the proposed scheme and the conventional Pragmatic TCM scheme is about 3.0 dB in the case of $error\ roof = 10^{-2}$ and 4.0 dB in the case of $error\ roof = 10^{-4}$. It can also be seen that the performance on the condition under $error\ roof = 10^{-4}$ is slightly better than that under $error\ \ roof = 10^{-2}$.

Figure 4.9 shows the total BER performance on the fading of $f_D T = 1.25 \times 10^{-5}$. The curves in this figure have the same trend as those in Fig. 4.8. In the area below Es/N0 = 12.5 dB, the performance of the proposed scheme is approximately the same as that of the conventional Pragmatic TCM scheme. At the BER = 10^{-4} level, the difference of the coding gain between the proposed scheme and the conventional Pragmatic TCM scheme is about 1.5 dB in the case of $error\ roof = 10^{-2}$ and 1.8 dB in the case where $error\ roof = 10^{-4}$. It is also shown that the performance under the condition of $error\ roof = 10^{-4}$ is slightly better than that under $error\ \ roof = 10^{-2}$.

Since the phase rotation is assumed to be ideally compensated in Figs.4.8 and 4.9, the BER performances become better as Es/N0 increases. If the rotation is not fully compensated, the BER may not decrease due to the error floor caused by each modulation scheme.

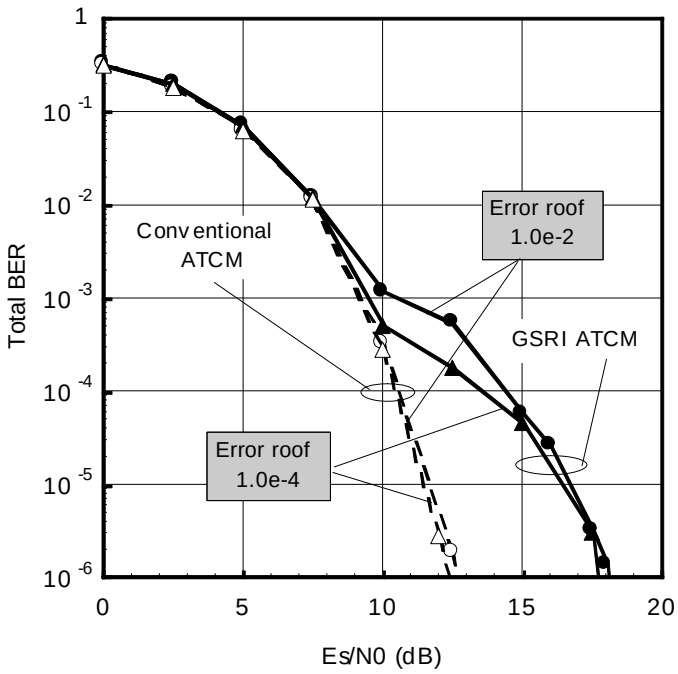

Fig. 4.8 Total BER performance of the proposed scheme and the conventional Pragmatic ATCM scheme on a multi-path fading channel ($f_D T = 1.56 \times 10^{-4}$)

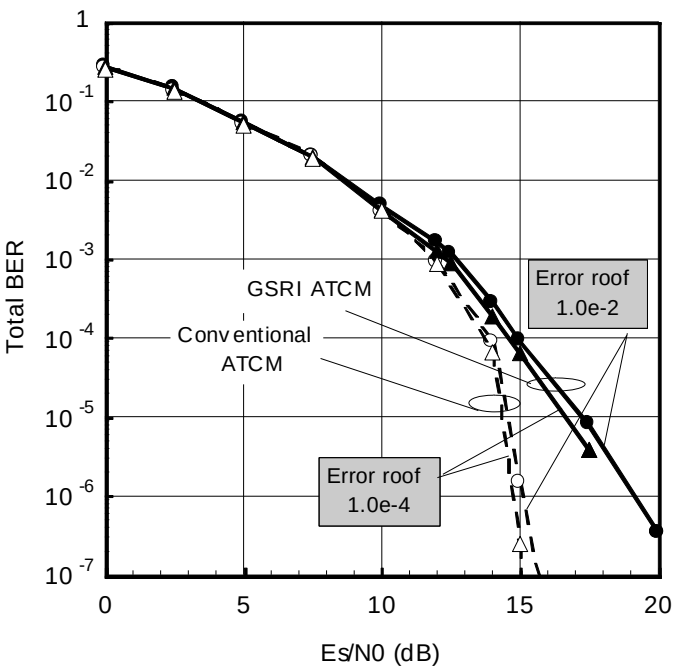

Fig. 4.9 Total BER performance of the proposed scheme and the conventional Pragmatic ATCM scheme on a multi-path fading channel ($f_D T = 1.25 \times 10^{-5}$)

4.4.3 Throughput performance

The frequency utilization efficiency described in Table 4.3 defines the transmitted information bits as sign bits. However, we need to consider how many information bits can be transmitted by both code selection bits and sign bits. The average throughput, η, in this case is defined as the number of bits transmitted in a modulation symbol per sub-carrier (bits/second/carrier) and can be derived as follows;

$$\eta = \frac{1}{n}\left(kq + \sum_{j=0}^{n-1} \overline{m}_j \right), \tag{4.2}$$

where $\overline{m}_j$ denotes the average number of input bits to the GSRI-TCM encoder # j .

Figure 4.10 compares the throughput performance between the proposed scheme and the conventional Pragmatic TCM scheme on the multi-path fading of $f_D T = 1.56 \times 10^{-4}$. In this figure, it is shown that the proposed scheme has better throughput performance than the conventional Pragmatic TCM scheme. The throughput performance under $error\ roof = 10^{-2}$ is higher than that under $error\ roof = 10^{-4}$ in the region from Es/N0 = 10 dB to 20 dB. Thismeans that more information bits are transmitted when the error roof is higher. There is a tradeoff between total BER and the throughput performance. The average improvement of the throughput for the proposed scheme compared with the conventional Pragmatic TCM scheme is 0.46 in both *error roof* cases. The throughput performance on the fading of $f_D T = 1.25 \times 10^{-5}$ is plotted in Fig. 4.11. This figure has the same trend as Fig. 4.10 in that the proposed scheme has better throughput performance than the conventional Pragmatic TCM scheme and the throughput performance for $error\ roof = 10^{-2}$ is higher than that of 10^{-4} in the region from Es/N0 = 7.5 dB to 20 dB. The average improvement in the throughput is obtained by 0.45 in the both *error roof* cases.

The presence of channel and SNR estimation errors caused by a noisy feedback channel, can lead to an incorrect selection of the modulation and coding schemes. In [67]-[68], the performance degradation affected by the estimation errors is analyzed. The performance of the practical adaptation threshold based on the channel estimation is considered in the next section.

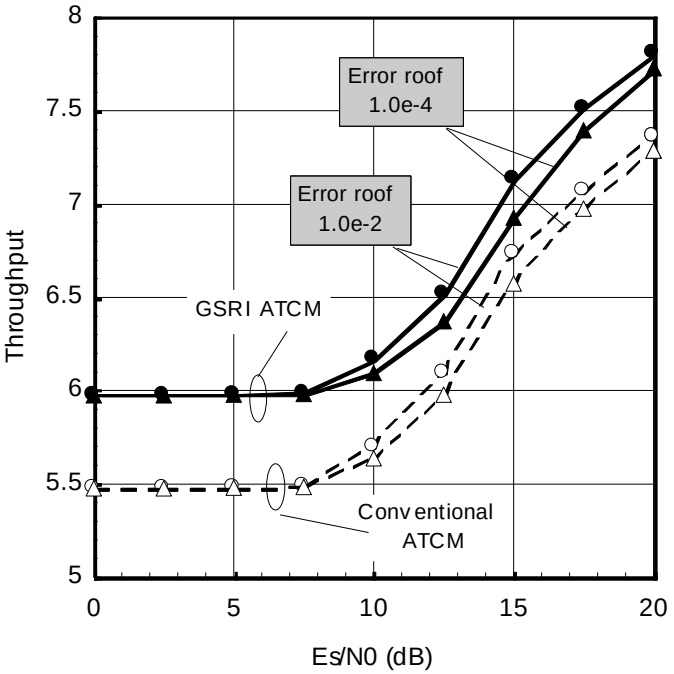

Fig. 4.10 Throughput of the proposed scheme and the conventional Pragmatic ATCM scheme on a multi-path fading channel ($f_D T = 1.56\times10^{-4}$)

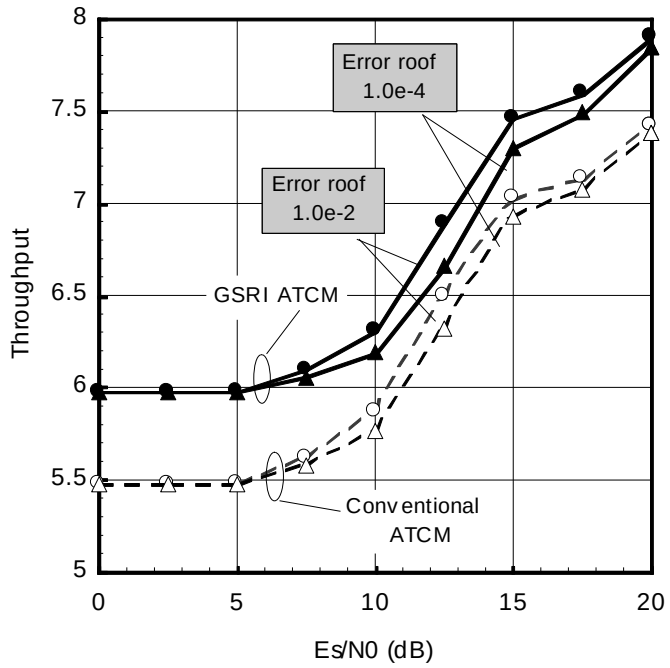

Fig. 4.11 Throughput of the proposed scheme and the conventional Pragmatic ATCM scheme on a multi-path fading channel ($f_D T = 1.25\times10^{-5}$ **)**

4.5 Modification of Adaptive Threshold Utilizing Practical Channel Estimation

In the evaluation in Section 4.4, the selection of the modulation and coding scheme for ATCM is assumed to be an ideal method described in [61]. However, since the modulation and coding selection are based on the ideal SNR estimation method, the adaptation thresholds are designed according to the BER performance on an AWGN channel and performance evaluations employing a practical channel estimation scheme are desired. In this section, an application of practical SNR estimation methods to the proposed scheme is considered. The performance of the adaptive modulation scheme including the effects of SNR estimation has been extensively studied [70]-[72]. Among the various studies, a simple and practical scheme using two pilot symbols is proposed in [70]. The proposed scheme applying this estimation method is considered. The BER and throughput performances are evaluated by simulations.

4.5.1 Estimation of Adaptive Threshold

The proposed system installs a frame format shown in Fig.4.12. In this figure, two pilot symbols are inserted before each *h* data symbol. These two pilot symbols are used for calculating the estimated noise power at the receiver. The pilot symbols consist of known pattern signals and are modulated by BPSK. In the frequency domain, the noise power of the channel can be obtained as follows:

$$P_n = \frac{1}{2N}\sum_{\ell=0}^{N-1}\left|\hat{s}_{\ell,1}^{p} - \hat{s}_{\ell,2}^{p}\right|^2 \tag{4.3}$$

where, $\hat{s}_{\ell,1}^{p}$ and $\hat{s}_{\ell,2}^{p}$ are the received signals for the ℓ th sub-carrier of the pilot symbols 1 and 2 at the output of the FFT module, respectively.

The received signal power for each sub-carrier can be estimated by the frequency response at the pilot tones and calculated as follows.

$$\hat{H}_{\ell} = (\hat{s}_{\ell,1}^{p} / s_{\ell,1}^{p} + \hat{s}_{\ell,2}^{p} / s_{\ell,2}^{p}) / 2 \tag{4.4}$$

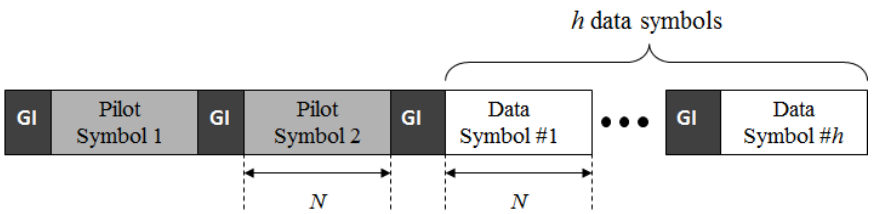

Fig. 4.12 Frame format

where, $\hat{H}_\ell$ is the frequency response for the ℓ th sub-carrier, and $s^p_{\ell,1}$ and $s^p_{\ell,2}$ are the transmitted signals for the ℓ th sub-carrier of the 1st and 2nd pilot symbols in the frequency domain, respectively. From eqs. (4.3) and (4.4), the estimated SNR for the ℓ th sub-carrier SNR_ℓ is given by

$$SNR_\ell = \frac{2^q}{q+1} \cdot \frac{\left|\hat{H}_\ell\right|^2}{P_n} \tag{4.5}$$

The modulation controller in Fig.1 decides the coding and modulation schemes for each sub-carrier based on the estimated SNR derived from eq.(4.5).

4.5.2 Evaluation Condition

The performances of the adaptive coding and modulations on multi-path fading channels are evaluated. The modulation and coding schemes listed in Table 4.3 are used, and simulation parameters are described in the Table 4.6. The performances on a two-path Rayleigh fading channel with DUR = 0.0 dB, (which is one of the severest channel models) are evaluated. To evaluate the basic performances, it is assumed that the receiver can detect the phase rotation of the received signal and is ideally compensated.

The same adaptation thresholds and the corresponding coding and modulation schemes listed in Table 4.5 are adopted. As stated in the previous section, the adaptation thresholds are chosen –by using the performance curves of individual schemes on the sign BER below an *error roof* on the fading channel. Figure 4.13 depicts this concept and is used for deciding the adaptation thresholds. When the *error roof* is set as BER = 10^{-2}, μ_1, μ_2, μ_3 and μ_4 are 11.1, 12.4, 14.2 and 18.9 dB, respectively.

Table 4.6 Simulation parameters on multi-path fading channels

(Pilot symbol based estimation of adaptation thresholds)

Sign bit Modulation	GSRI Pragmatic ATC-MPSK Conv. Pragmatic ATC-MPSK
RS Coding	(15,7)RS code
Hadamard code	h=16
Number of FFT (Number of sub-carriers)	N=16
Fading Model	2-path Rayleigh fading DUR=0.0dB $f_D T$= 2.0X10^{-4}
Delay Spacing	τ_d/T_s =6.25X10^{-2} (τ_d :path delay, T_s :OFDM symbol duration)
Guard Interval	T_g=0.25T_s
Channel Estimation	Perfect channel estimation
Adaptation Threshold	Pilot symbol based estimation

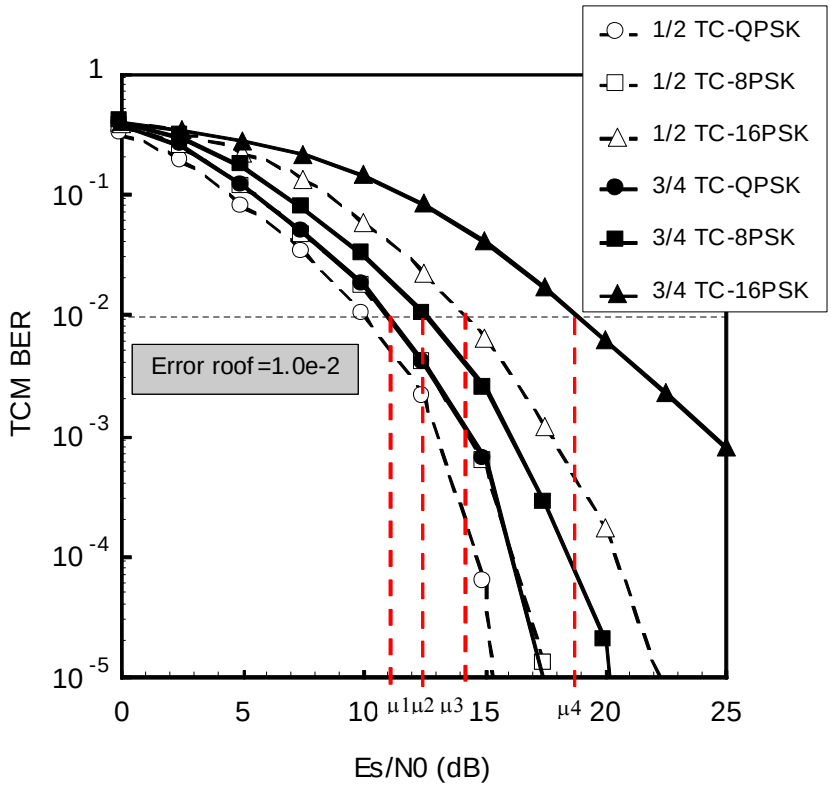

Fig. 4.13 Sign bit error rate on a multi-path fading channel

4.5.3 Performance Evaluation

The total BER performances of the proposed scheme and the conventional Pragmatic TCM scheme on the multi-path fading are shown in Fig. 4.14. In this figure, the *error roof* is set to be BER = 10^{-2}. Comparing the performance of the proposed scheme with that of the conventional Pragmatic TCM scheme, it is shown that the BER performance is approximately the same as that in the region where $E_s / N_0 \leq 10$ dB. When Es/N0 is higher than 10 dB, the conventional Pragmatic TCM scheme performs better than the proposed scheme. This is because that the conventional Pragmatic TCM scheme chooses only the coding rate of the r = 1/2 case for each modulation scheme and this parameter selection keeps the BER lower than that of the proposed scheme. Figure 4.15 compares the throughput performance between the proposed scheme and the conventional Pragmatic TCM scheme calculated from eq. (4.2) on the multi-path fading channel. This figure shows that the proposed scheme has better throughput performance than the conventional Pragmatic TCM scheme. There is a tradeoff between the total BER and the throughput performance.

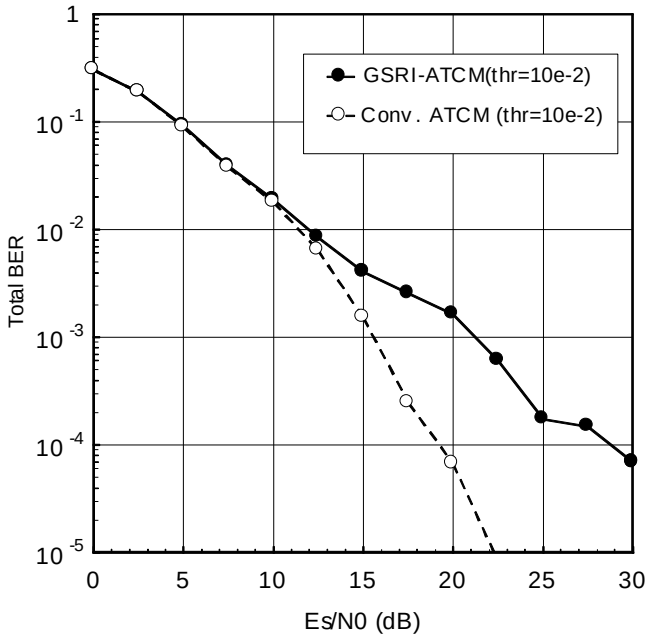

Fig. 4.14 Total BER performance of the proposed scheme and

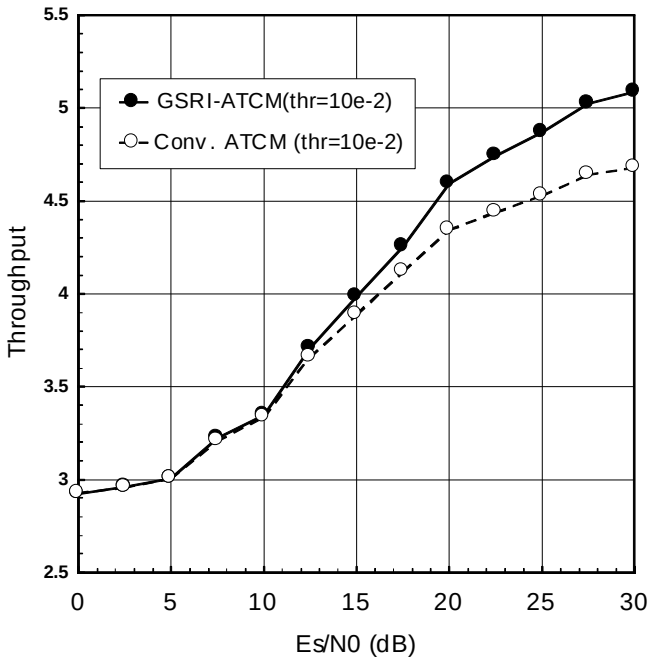

Fig. 4.15 Throughput performance of the proposed scheme and the conventional Pragmatic ATCM scheme on a multi-path

4.6 Simplified Transmitter Structure and its Performance

4.6.1 Simplified Transmitter Structure

The simplified transmitter structure is shown in Fig.4.16. In this figure, the incoming binary bits are serial-to-parallel converted into $kq+mn$ parallel bit streams, where k is the number of input sequences to the RS encoder and q is the number of bits in each input sequence. These k input sequences are fed into the (n,k)RS encoder over GF(2^q). The encoded symbols are input into n code selection modules and each module selects an orthogonal code. In the code-selection module, the orthogonal code used is the Hadamard code. When a q bit symbol of an RS codeword is fed into the modulator, one of the h Hadamard codewords is selected. On the other hand, mn parallel sign bit signals are encoded and modulated by a GSRI-TCM module into n parallel codewords and are input into n Hadamard encoders for spreading. Here, m denotes a GSRI-TCM encoder input bit and its value is determined by the selected coding rate and modulation scheme. The modulated sequences are fed into the interleaver and are randomized by a random interleaver. The number of the interleaver input signal is the same as in the N point IFFT.

The difference from the original GSRI-ATCM (hereinafter called the adaptive scheme) is that the number of GSRI-ATCM encoders is reduced to one. Additionally, the modulation controller has a different algorithm for setting the coding rate and modulation scheme. The adaptive scheme optimally selects the coding rate and modulation scheme for each sub-carrier according to its estimated SNR [70]. In the simplified model, the modulation parameter of the simplified scheme is derived by averaging the estimated SNRs of sub-carriers and all the sub-carriers are set to the same coding rate and modulation scheme. This average SNR is calculated as follows:

$$SNR_{av} = \frac{1}{N}\sum_{\ell=0}^{N-1} SNR_{\ell} \quad , \tag{4.6}$$

where N and SNR_{ℓ} denote the number of FFT and the estimated SNR for sub-carrier $\#\ell$ ($0 \le \ell \le N-1$), respectively.

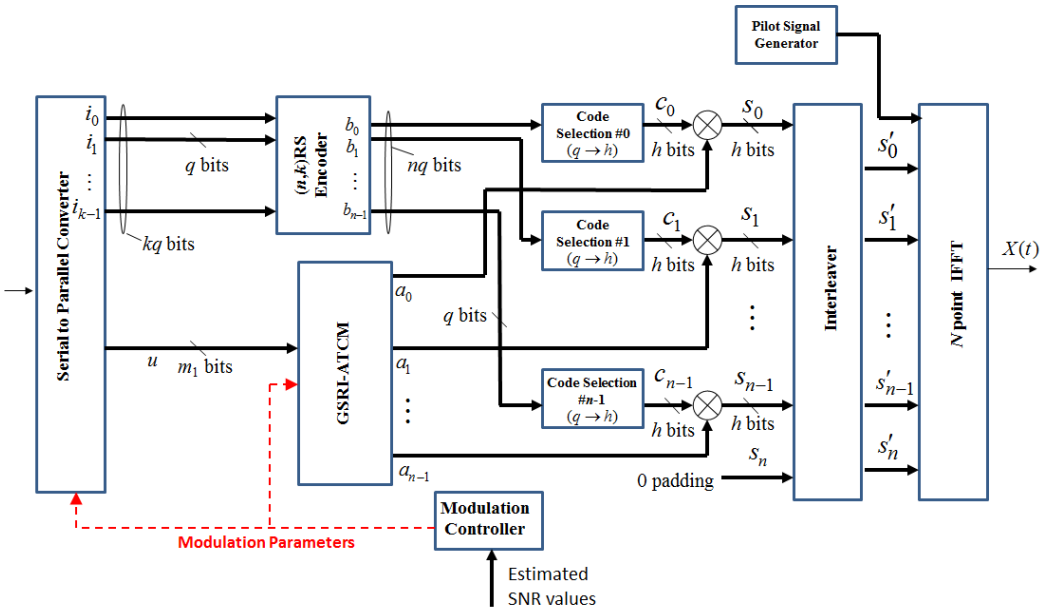

Fig.4.16 Simplified transmitter structure

The coding rate and modulation scheme are selected how high the SNR_{av} is obtained. The adaptation thresholds, coding rate, and modulation scheme applied in this case are shown in Table 4.7, where the selection policy is the same as those given in Table 4.5. In this table, the full adaptive scheme selects the optimal coding rate and modulation scheme for each sub-carrier. On the other hand, the simplified scheme selects a coding rate and modulation scheme for all sub-carriers according to the value of SNR_{av}. The adaptation thresholds μ_1, μ_2, μ_3 and μ_4 are given by an experimental evaluation [73].

The average throughput, η, for the simplified scheme is defined as the number of bits transmitted in a modulation symbol per sub-carrier (bits/second/carrier) and can be derived as follows:

$$\eta = \frac{kq}{n} + \overline{m}\,, \tag{4.7}$$

where $\overline{m}$ denotes the average number of input bits to the GSRI-TCM encoder.

Table 4.7 Adaptation thresholds
(Simplified and adaptive schemes)

Adaptation threshold	Simplified scheme	Adaptive scheme
r=1/2 TC-QPSK	$SNR_{av} < \mu_1$	$SNR_\ell < \mu_1$
r=3/4 TC-QPSK	$\mu_1 \le SNR_{av} < \mu_2$	$\mu_1 \le SNR_\ell < \mu_2$
r=3/4 TC-8PSK	$\mu_2 \le SNR_{av} < \mu_3$	$\mu_2 \le SNR_\ell < \mu_3$
r=1/2 TC-16PSK	$\mu_3 \le SNR_{av} < \mu_4$	$\mu_3 \le SNR_\ell < \mu_4$
r=3/4 TC-16PSK	$\mu_4 \le SNR_{av}$	$\mu_4 \le SNR_\ell$

4.6.2 Performance Evaluation

The performance of the simplified scheme on a multi-path fading channel is evaluated. The simulation parameters are listed in Table 4.6. The (15,7) RS code is employed and then the number of FFTs is 16. The performance on a two-path Rayleigh fading channel with DUR = 0 dB is evaluated. To evaluate the basic performance, it is assumed that the phase rotation is compensated at the receiver.

In the simplified scheme, the coding rate and modulation scheme are selected according to the adaptation thresholds μ_1, μ_2, μ_3 and μ_4 in Table 4.7. These values are set to 11.1, 12.4, 14.2 and 18.9 dB, respectively. These are given by the BER performance for each combination of the coding rate and modulation scheme shown in Fig. 4.13. In this figure, the adaptation thresholds are set such that the *error roof* is 10^{-2} [73].

Figure 4.17 shows the BER performance of the simplified scheme compared with the adaptive scheme. In this figure, the performance of the simplified scheme is slightly degraded compared to that of the adaptive scheme. Since a single encoder and decoder are employed in the simplified scheme, all of the sub-carriers have the same coding rates and modulation schemes. The modulation parameter is not optimized along with the channel condition and the BER performance is not optimally achieved, either. The selected coding rate and modulation scheme based on SNR_{av} are inclined to be better channel conditions than those based on the adaptive scheme. Figure 4.18 shows the throughput performance of the simplified and adaptive schemes. In this figure, the simplified scheme achieves higher throughput performance than the adaptive scheme. This trend is also caused by the same

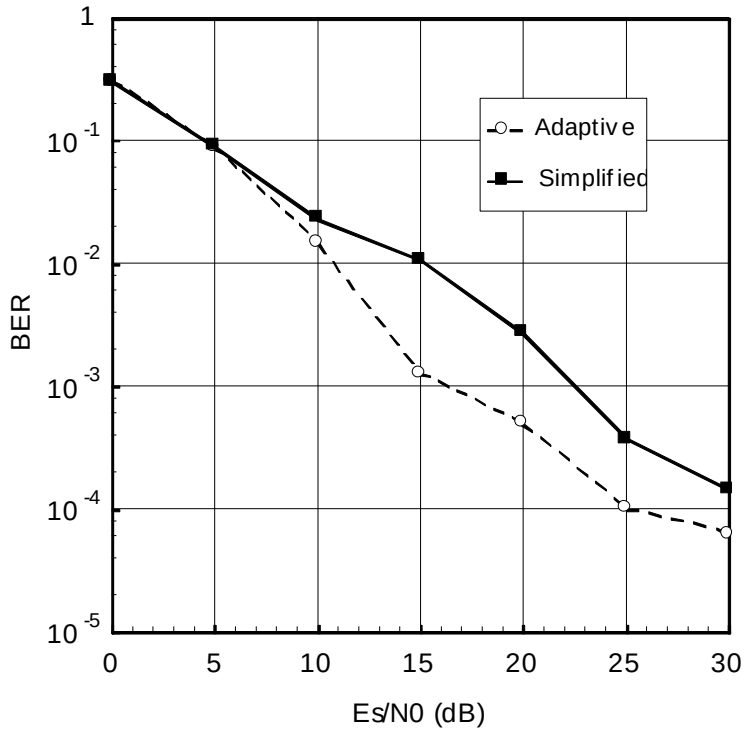

Fig.4.17 Total BER performance of the simplified scheme and the adaptive scheme

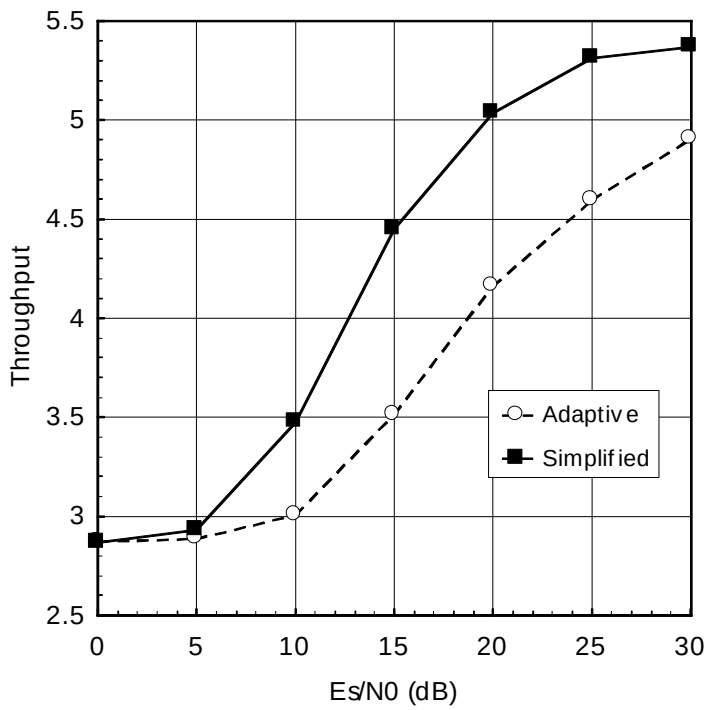

Fig.4.18 Throughput of the simplified scheme and the adaptive scheme

reason. Since the BER performance and throughput have a tradeoff, the simplified scheme has a higher throughput performance compared with the adaptive scheme.

4.7 Conclusion

This chapter has proposed an application of GSRI Pragmatic ATC-MPSK to RS coded MC-DS-CDMA with bi-orthogonal keying. First o, the general construction of the GSRI ATCM for the RS coded MC-DS-CDMA with a bi-orthogonal keying system was presented. Then the BER performances on an AWGN channel and multi-path fading channels were evaluated by simulations. We have also defined the throughput for this system and compared the throughput performance between the proposed scheme and the conventional Pragmatic ATCM scheme. It was shown that the BER performance for both schemes had approximately the same performance in the area of lower Es/N0 and that the BER of the conventional Pragmatic TCM scheme improved more than that of the proposed scheme in the higher Es/N0 region. However, the proposed scheme obtained remarkably higher throughput performance than the conventional Pragmatic TCM scheme. The throughput of the schemes using larger *error roof*s was better than those with smaller ones.

We also employed a practical SNR estimation scheme using two pilot symbols and the performances on a multi-path fading channel were evaluated. It was clarified that the performance trend was the same as that for ideal SNR estimation. It was also shown that the adaptive threshold could be designed according to the BER performances on fading channels. This can be used to model the modulation controller performance.

Finally, a simplified encoder/decoder structure was investigated. The simplified scheme could remarkably reduce the complexity: however, the BER performance was slightly degraded. This implies that there was a tradeoff between BER performance and encoder/decoder complexity. The simplified scheme showed better performance than the adaptive scheme because of coding rate and modulation scheme was less optimized. The SNR_{av} approach was one of the basic investigations.

Chapter 5

Conclusions

This thesis has presented a reliable video transmission scheme. To achieve high reliability, the following two approaches were proposed. The first one was an enhanced error resilient video coding and the second one was an efficient error control coding for an adaptive trellis coded MC-DS-CDMA system. The first approach was described in Chapter 2 and the second approach was considered in Chapters 3 and 4.

In Chapter 2, an enhanced spatial and temporal EC method for a 3 D DWT video coding scheme was proposed to achieve higher performance in packet loss networks. In our previous papers we studied a two-step EC method consisting of a DG of the lowest frequency pixels and their duplication of transmission. In the enhancement to a temporal EC method, the SSIM index was used for inter GOP EC and MMSE was used for intra-GOP EC. The SSIM index was used for measuring the similarity between two frames. In the inter GOP EC, the similarity of the lowest sub-band frames between neighboring GOPs was high. Since the SSIM index could reflect perceptual distortions, it could represent the visual quality accurately. The proposed method could first recover packet errors using a spatial EC method with spatiotemporal low-frequency sub-band duplication information, and then the video decoder could recover erroneous video frames from spatially and temporally adjacent coefficients. The simulation results revealed the proposed EC method obtained better performance compared with the conventional two-step EC method. It was also shown that the proposed method achieved remarkable improvement for relatively slow motion video sequences.

In Chapter 3, an error correction scheme suitable for an MC-DS-CDMA system with bi-orthogonal modulation was proposed. To employ an efficient error coding, the coding conditions

for this system were clarified. Based on these conditions, the following coding scheme was proposed: applying the RS code for selection bits and no error correction code with demodulator modification for sign bits. The code-selection error and BER performance on an AWGN channel were evaluated by theoretical analysis and simulations, and simulation results on multi-path fading channels were also provided. It was shown that the proposed scheme obtained remarkable improvements over uncoded schemes. Compared with a convolutional coding scheme, the proposed scheme could achieve higher performances.

In Chapter 4, an application of GSRI Pragmatic ATCM to RS coded MC-DS-CDMA with bi-orthogonal keying was proposed. A general transmitter and receiver structure of the GSRI ATCM for the RS coded MC-DS-CDMA with a bi-orthogonal keying system was presented. Then the BER performances on an AWGN channel and multi-path fading channels were evaluated. We have also defined the throughput for this system and compared the throughput performance between the proposed scheme and the conventional Pragmatic ATCM scheme. It was clarified that the application of the proposed GSRI Pragmatic ATCM has effective in terms of both BER performance and throughput performance and that the proposed scheme could increase the frequency utilization efficiency.

Therefore, this thesis contributes to the building of a reliable wireless video transmission system that achieves high robustness against error prone channels.

However, there still remain challenges for further study. In the proposed spatial and temporal error concealment method, an efficient method for relatively fast motion video sequences should be further investigated. In the GSRI-ATCM MC-DS-CDMA, the simplified scheme can remarkably reduce the complexity: however, the BER performance is slightly degraded. The evaluation in this thesis was an example of basic approaches and a more appropriate method should be considered.

Finally, I hope that the research results of this thesis contribute to the progress of information science.

Achievement

Papers

(A) **Journal Papers**

[A-1] Hirokazu Tanaka, Kyung-Wung Jang, Shoichiro Yamasaki and Miki Haseyama, 'Performance of Reed-Solomon Coded MC-DS-CDMA with Bi-orthogonal Modulation,' IEICE Transactions on Fundamentals, Vol.E92-A, pp.2600-2608, Oct. 2009.

[A-2] Hirokazu Tanaka, Shoichiro Yamasaki and Miki Haseyama, 'Performance of Adaptive Trellis Coded Modulation Applied to MC-CDMA with Bi-orthogonal Keying,' IEICE Transactions on Fundamentals, Vol.E92-A, pp.2837-2843, Nov. 2009.

[A-3] Hirokazu Tanaka, Sunmi Kim, Takahiro Ogawa and Miki Haseyama, 'Performance of Spatial and Temporal Error Concealment Method for 3D DWT Video Coding in Packet Loss Channel,' IEICE Transactions on Fundamentals, to be published in Vol.E95-A, pp.2015-2022, Nov. 2012.

(B) **International Conference**

[B-1] Hirokazu Tanaka, Shoichiro Yamasaki and Miki Haseyama, 'Error Correction Scheme for Multi-carrier CDMA with Bi-orthogonal Modulation,' Proc. International Symposium on Information Theory and Its Applications (ISITA), #342, pp.1061-1066, Dec. 2008.

[B-2] Hirokazu Tanaka, Shoichiro Yamasaki and Miki Haseyama, 'Performance of Adaptive Modulation and Coding (AMC) on Multi-carrier CDMA for Mobile Multimedia Transmission,'

Proc. IEEE Int. Sym. on Broadband Multimedia Systems and Broadcasting (BMSB), mm09-178, pp.1-5, May. 2009.

[B-3] Hirokazu Tanaka, S.Yamasaki and M.Haseyama, ‘A Study on Multi-carrier CDMA with Adaptive Trellis Coded Modulation,’ Proc. IEEE International Symposium on Intelligent Signal Processing and Communication Systems (ISPACS 2009), WA2-A-5,pp.477-480, Dec. 2009.

[B-4] Hirokazu Tanaka, Shoichiro Yamasaki, Tomoko K. Matsushima and Miki Haseyama,’ A Study on Simplified Structure for Multi-carrier DS-CDMA with bi-orthogonal keying,’ Proc. International Technical Conference on Circuits/Systems, Computers and Communications (ITC-CSCC) 2014,PID1063, pp.100-102, Jul. 2014.

Bibliography

[1] D. Gómez-Barquero, Next Generation Mobile Broadcasting, CRC Press, 2013

[2] L.Dai, Z.Wang and Z.Yang, 'Next-Generation digital television terrestrial broadcasting systems: Key technologies and research trends,' IEEE Comm. Mag., Vol. 50, No.6, pp.150-158, Jun. 2012.

[3] T.Wiegand and G.J.Sullivan, 'The H.264/AVC video coding standard,' IEEE Signal Processing Magazine, vol. 24, no. 2, pp. 148-153, Mar. 2007.

[4] 'Information technology−Generic coding of moving pictures and associated audio information: Video,' ISO/IEC 13818-2, MPEG-2 Video Coding Standard, 1995.

[5] 'Information technology−Coding of audio-visual objects−Part 2: Visual,' ISO/IEC 14496-2, MPEG-4 Coding Standard, 1999.

[6] G.J.Sullivan, J-R.Ohm, W-J.Han and T.Wiegand, 'Overview of the high efficiency video coding (HEVC) standard,' IEEE Transactions on Circuits and Systems for Video Technology, Vol.22, No.12, pp.1649-1668, Dec. 2012.

[7] K.Yoshida, K.Izumi, H.Yoshida, R.Miura and F.Ono, 'Demands on Reliable and Robust Wireless Communications under Land-Sea-and-Air Extreme Environments,' IEICE Transactions on Fundamentals, Vol. E96-A, No. 5, pp.844-852, May 2013.

[8] S.Blackburn, S.Brownsell and M.S.Hawley. 'A Systematic review of digital interactive television systems and their applications in the health and social care fields,' Journal of Telemedicine and Telecare, Vol. 17, No. 4, pp.168-176, Jun. 2011.

[9] J.Lloret, A.Canovas, S.Sendra and L.Parra, 'A smart communication architecture for ambient assisted living,' IEEE Communications Magazine, Vol.53, No.1, pp.26-33, Jan. 2015.

[10] S.Spinsante and E.Gambi, 'Remote health monitoring by OSGi technology and digital TV integration,' IEEE Transactions on Consumer Electronics, Vol.58, No.4, pp.1434-1441, Nov. 2012.

[11] J.C.Kim, D.Y.Kim, S.M.Jung, M.H.Lee, K.S.Kim, C.K.Lee, J.Y.Nah, S.H.Lee, J.H.Kim, W.J.Choi and S.K.Yoo, 'Implementation and performance evaluation of mobile ad hoc network for emergency telemedicine system in disaster areas, ' Proc. IEEE International Conference of the Engineering in Medicine and Biology Society (EMBS), pp.1663-1666, Sep. 2009.

[12] T.Sheltami, A.Al-Roubaiey, E.Shakshuki and A.Mahmoud, 'Video transmission enhancement in presence of misbehaving nodes in MANETs,' Springer Multimedia Systems, Vol.15, No.5, pp.273-282, Oct. 2009.

[13] W.Hamidouche, R.Vauzelle, C.Olivier, Y.Pousset and C.Perrine, 'Impact of realistic MIMO physical layer on video transmission over mobile Ad Hoc network,' Proc. IEEE International Symposium on Personal, Indoor and Mobile Radio Communications (PIMRC), pp.187-191, Sep. 2009.

[14] S.Hara and R.Prasad, 'Overview of Multicarrier CDMA,' IEEE Communications Magazine, pp.126-133, Dec.1997.

[15] E.A.Sourour and M.Nakagawa, 'Performance of orthogonal multicarrier CDMA in a multipath fading channel,' IEEE Transactions on Communications, vol. 44, pp. 356-366, Mar. 1996.

[16] F.Adachi, D.Garg, S.Takaoka and K.Takeda, 'Broadband CDMA Techniques,' IEEE Wireless Communications, pp.8-18, Apr. 2005.

[17] R.Caldwell and A.Anpalagan, 'Meeting mobile's demands with multicarrier systems,' IEEE Potentials, vol.24, no.5, pp. 27-31, Dec. 2005.

[18] K.Fazel and S.Kaiser, Multi-Carrier and Spread Spectrum Systems: from OFDM and MC-CDMA to LTE and WiMAX, John Wiley & Sons Inc., 2008.

[19] A.S.Bahai and B.R.Saltzberg, Multi-Carrier Digital Communications, Kluwer Academic Pub., 1999.

[20] L.L.Yang and L.Hanzo, 'Multicarrier DS-CDMA: A Multiple Access Scheme for Ubiquitous Broadband Wireless Communications,' IEEE Communications Magagine, pp.116-124, Oct. 2003.

[21] S.B.Weinstein, 'Introduction to the History of OFDM,' IEEE Communications Magazine, Vol. 47, No.11, Nov. 2009.

[22] L.Yang and E.Alsusa, 'Dynamic Code-allocation Based PAPR Reduction Technique for MC-CDMA Systems,' Proc. IEEE Wireless Communications & Networking Conference (WCNC), pp.628-633, Mar.2007.

[23] Y-H.You, W-G.Jeon, B-C,Song and H-K.Jung, ‘Reducing Peak-to-average Power Ratio Using Transformed CDMA/OFDM Signals,’ IEE Electronics Letters Vol.39, No.4, pp.403-405, Feb. 2003.

[24] S.H.Han and J.H.Lee, ‘An Overview of Peak-To-Average Power Ratio Reduction Techniques for Multicarrier Transmission,’ IEEE Wireless Communications, pp.56-65, Apr. 2005.

[25] T.Jiang and Y.Wu, ‘An Overview: Peak-to-Average Power Ratio Reduction Techniques for OFDM Signal,’ IEEE Transactions on Broadcasting, Vol.54, No.2, pp.257-268, Jun. 2008.

[26] X.Dai, J.Liang , H.Wu and D.Li, ‘An Effective Method for PAPR Reduction in MC-DS-CDMA Systems,’ Proc. International Conference on Wireless Communications, Networking and Mobile Computing (WiCOM), 102, pp.1-4, Sep. 2006.

[27] H. Schwarz, D. Marpe, and T. Wiegand ‘Overview of the scalable video coding extension of the H.264/AVC standard,’ IEEE Transactions on Circuits and Systems for Video Technology, vol. 17, no. 9, pp. 1103-1120, Sept. 2007.

[28] N. Adami, A. Signoroni and R. Leonardi, ‘State-of-the-art and trends in scalable video compression with wavelet-based approaches,’ IEEE Transactions on Circuits and Systems for Video Technology, vol. 17, no. 9, pp. 1238-1255, Sept. 2007.

[29] B.-J. Kim, Z. Xiong, and W. Pearlman, ‘Low bit-rate scalable video coding with 3D set partitioning in hierarchical trees (3D SPIHT),’ IEEE Transactions on Circuits and Systems for Video Technology, vol. 10, no. 8, pp. 1374-1387, Dec. 2000.

[30] C. He, J. Dong, Y. Zheng, and Z. Gao, ‘Optimal 3-D coefficient tree structure for 3-D wavelet video coding,’ IEEE Transactions on Circuits and Systems for Video Technology, vol. 13, no. 10, pp. 961-972, Oct. 2003.

[31] Y. Wang and Q. F. Zhu, ‘Error control and concealment for video communication: A review,’ Proceedings of the IEEE, vol. 86, no. 5, pp. 974-997, May 1998.

[32] J. M. Shapiro, ‘Embedded image coding using zerotrees of wavelet coefficients,’ IEEE Transactions on Signal Processing, vol. 41, no. 12, pp. 3445–3463, Dec. 1993.

[33] A. Said and W. A. Pearlman, ‘A new, fast, and efficient image codec based on set partitioning in hierarchical trees,’ IEEE Transactions on Circuits and Systems for Video Technology, vol. 6, no. 3, pp. 243–250, June 1996.

[34] V. K. Goyal, ‘Multiple Description Coding: Compression meets the network,’ IEEE Signal Processing Magazine, vol. 18, no. 5, pp. 74 -94, Sept. 2001.

[35] T. Kim, S. Choi, R. E. Van Dyck, and N. K. Bose, ‘Classified zerotree wavelet image coding and adaptive packetization for low-bit-rate transport,’ IEEE Transactions on Circuits and Systems for Video Technology, vol. 11, no. 9, pp. 1022–1034, Sep. 2001.

[36] F. Verdicchio, A. Munteanu, A. I. Gavrilescu, and P. Schelkens, ‘Embedded multiple description coding of video,’ IEEE Transactions on Image Processing, vol. 15, no. 10, pp. 3114-3130, Oct. 2006.

[37] I. V. Bajic and J. W. Woods, ‘Domain-based multiple description coding of images and video,’ IEEE Transactions on Image Processing, vol. 12, no. 10, pp. 1211-1225, May 2003.

[38] J. Rombaut, A. Pizurica, and W. Philips, ‘Optimization of packetization masks for image coding based on an objective cost function for desired packet spreading,’ IEEE Transactions on Image Processing, vol. 18, no. 4, pp. 783-796, Apr. 2009.

[39] S. Cho and W. A. Pearlman, ‘A full-featured, error-resilient, scalable wavelet video codec based on the set partitioning in hierarchical trees (SPIHT) algorithm,’ IEEE Transactions on Circuits and Systems for Video Technology, vol. 12, no. 3, pp. 157-171, Mar. 2002.

[40] Y. G. Wu and C. H. Wu, ‘Image vector quantization indices recovery using Lagrange interpolation,’ in Proc. IEEE International Conference on Multimedia and Expo (ICME 2006), pp. 1197-1200, Jul. 2006.

[41] I. V. Bajic, ‘Adaptive MAP error concealment for dispersively packetized wavelet-coded images,’ IEEE Transactions on Image Processing, vol. 15, no. 5, pp. 1226- 1235, May 2006.

[42] J. Rombaut, A. Pizurica, and W. Philips, ‘Passive error concealment for wavelet-coded I-frames with an inhomogeneous Gauss–Markov random field model,’ IEEE Transactions on Image Processing, vol. 18, no. 4, pp. 783-796, Apr. 2009.

[43] S. Kim, H. Tanaka, T. Ogawa and M. Haseyama, ‘Two-step error concealment method for 3-D wavelet video coding in wireless packet transmission system,’ in Proc. International Technical Conference on Circuits, System, Computers and Communications (ITC-CSCC 2010), pp. 500-503, Jul. 2010.

[44] ITU-T H.222.0, ‘Generic coding of moving pictures and associated audio information: Systems’, May 2006.

[45] S. Kim, H. Tanaka, T. Ogawa and M. Haseyama, ‘Error-resilient 3-D wavelet video coding with duplicated lowest sub-band coefficients and two-step error concealment method,’ IEICE Transactions on Fundamentals, vol. E93-A, no. 11, pp. 2173-2183, Nov. 2010.

[46] X.Xu, B.Bai, Y.Cai,X.Qiao and R.Zhu, ‘A M-ary Biorthogonal Code SS Multicarrier CDMA Transmission Sceme,’ Proc. IEEE International Conference on Neural Networks & Signal Processing, pp.667-671, Dec. 2003.

[47] J.K.Hwang, Y.L.Chiu and R.L.Chung, ‘A New Class of MC-CDMA Systems Using Cyclic-Shift M-ary Biorthogonal Keying,’ Proc. International Symposium on Intelligent Signal Processing and Communications Systems (ISPACS), pp.67-70, Dec. 2006.

[48] D.J.Costello, J.Hagenauer, H.Imai and S.B.Wicker, ‘Applications of Error-Control Coding,’ IEEE Transactions on Information Theory, vol.44, no.6, pp.2531-2560, Oct. 1998.

[49] ISO/IEC 8802.11:1999/Amd1:2000(E), Wireless LAN Medium Access Control (MAC) and Physical Layer (PHY) Specifications, Jun. 2003.

[50] W.Bocquet, K.Hayashi and H.Sakai, ‘A Novel Power Distribution Scheme Combined with Adaptive Modulation Based on Subcarrier Grouping for OFDM Systems,’ IEICE Transactions on Communications, Vol.E91-B, no.12, pp.3974-3982, Dec.2008.

[51] S.S.Das, F.Tariq, M.I.Rahman, F.B.Frederiksen, E.D.Carvalho and R.Prasad, ‘Impact of Nonlinear power Amplifier on Link Adaptation Algorithm of OFDM Systems,’ Proc. IEEE Vehicular Technology Conference (VTC) Fall, pp.1303-1307, Sep. 2007.

[52] K.Ohuchi, ‘Proposal of a Convolutional Coding Method for DS/SS Systems with M-ary Bi-Orthogonal Keying,’ Proc. IEEE International Symposium on Spread Spectrum Techniques and Applications (ISSSTA), pp.295-299, Aug. 2004.

[53] Z. Wang, A. C. Bovik, H. R. Sheikh and E. P. Simoncelli, ‘Image quality assessment: From error visibility to structural similarity,’ IEEE Transactions on Image Processing, vol. 13, no. 4, pp. 600-612, Apr. 2004.

[54] T.Zhao, J.Wang, Z.Wang and C.W.Chen, ‘SSIM-Based Coarse-Grain Scalable Video Coding,’ IEEE Transactions on Broadcasting, vol.61, No.2, pp.210-221, Jun. 2015.

[55] S.B.Wicker and V.K.Bhargava, Reed-Solomon Codes and Their Applications, IEEE Press, Piscataway, NJ, 1994.

[56] S.Lin and D.J.Costello, Error Control Coding, Pearson Education International, Inc., 2004.

[57] Y.Teng, T.Nagaosa, K.Mori and H.Kobayashi, ‘Proposal of Grouping Adaptive Modulation Method for Burst Mode OFDM Transmission System,’ IEICE Transactions on Communications, Vol.E86-B, No.1, pp.257-265, Jan. 2003.

[58] W.Bocquet, K.Hayashi and H.Sakai, ‘A Novel Power Distribution Scheme Combined with Adaptive Modulation Based on Subcarrier Grouping for OFDM Systems,’ IEICE Transactions on Communications, Vol.E91-B, No.12, pp.3974-3982, Dec.2008.

[59] H.Tanaka and S.Yamasaki: ‘Pragmatic Trellis Coded MPSK with Bandwidth Expansion on Rayleigh Fading Channels,’ IEICE Transactions on Communications, Vol.E81-B, No.12, pp.2276-2282, Dec. 1998.

[60] A.J.Viterbi, J.K.Wolf, F.Zehavi and R.Padovani; ‘A Pragmatic Approach to Trellis-coded Modulation,’ IEEE Communications Mag., pp.11-19, July 1989.

[61] S. M. Alamouti and S. Kallel, ‘Adaptive Trellis-Coded Multiple-Phase-Shift Keying for Rayleigh Fading Channels,’ IEEE Transactions on Communications, Vol.42, No.6, pp.2305-2314, Jun. 1994.

[62] Z.Wang, A.C.Bovik, H.R.Sheikh and E.P.Simoncelli, ‘Image quality assessment: From error visibility to structural similarity,’ IEEE Transactions on Image Processing, vol.13, no.4, pp.600-612, Apr. 2004.

[63] B.Girod, ‘What’s wrong with mean-squared error?,’ in Digital Images and Human Vision, A.B.Watson, *Ed.* Cambridge, MA: MIT Press, 1993, pp.207-220.

[64] H.R.Sheikh, M.F.Sabir and A.C.Bovik, ‘A statistical evaluation of recent full reference image quality assessment algorithms,’ IEEE Transactions on Image Processing, vol.15, no.11, pp.3440-3451, Nov.2006.

[65] M.J.Kim, S.P.Kim, and J.W.Cho, ‘A Multi-Code Biorthogonal Code Keying with Constant Amplitude coding’, IEICE Transactions on Communications, vol.E88-B, no.7, pp.2928-2936, Jul.2005.

[66] W.C. Lindsey and M.K.Simon, Telecommunication System Engineering, Prentice-Hall, 1973.

[67] J.G.Proakis, Digital Communications, McGraw-Hill Companies, Inc., 2001.

[68] J.Yun, W.Jeong and M.Kavehrad, ‘Throughput Analysis of Selective Repeat ARQ Combined with Adaptive Modulation for Fading Channels,’ Proc. IEEE Military Communications Conference (MILCOM), pp.710-714, Oct. 2002.

[69] A.J.Goldsmith, L.J.Greenstein and G.J.Foschini, ‘Error Statistics of Real-time Power Measurements in Cellular Channels with Multipath and Shadowing,’ Proc. IEEE Transactions on Vehicular Technology, vol.43, No.3, pp.439-446, Aug. 1994.

[70] Y.Teng, T.Nagaosa, K.Mori and H.Kobayashi, ‘Proposal of Grouping Adaptive Modulation Method for Burst Mode OFDM Transmission System,’ IEICE Transactions on Communications, Vol.E86-B, No.1, pp.257-265, Jan. 2003.

[71] J.M.Torrance and L.Hanzo, ‘Optimisation of switching levels for adaptive modulation in slow Rayleigh fading,’ IEE Electronics Letters, Vol.32, No.13, pp.1167-1169, Jun. 1996.

[72] J.F.Paris, M.C.Aguayo-Torres and J.T.Entrambasaguas, ‘Impact of Channel Estimation Error on Adaptive Modulation Performance in Flat Fading,’ IEEE Transactions on Communications, Vol.52, No.5, pp.716-720, May 2004.

[73] H.Tanaka, S.Yamasaki, M.Haseyama,’A Study on Multi-carrier CDMA with Adaptive Trellis Coded Modulation,’ Proc. International Symposium on Intelligent Signal Processing and Communication Systems (ISPACS2009), pp.477-480, Dec. 2009

Acknowledgements

I would like to express my deep sincere gratitude to my supervisor, Professor Miki Haseyama. Her extensive knowledge and logical way of thinking have been of great value to me. Her understanding, encouragement and personal guidance have provided a good basis for my thesis. Her guidance was very important to this study; without her valuable advice and friendly assistance, this study would not have been completed easily.

I would like to thank Professor Tsuyoshi Yamamoto, Professor Kenji Araki, and Professor Yuji Sakamoto for reviewing my thesis and providing insightful comments and suggestions.

I am very grateful to Assistant Professor Takahiro Ogawa for his constant encouragement and many fruitful discussions about this study. This thesis would not have been possible without his help, support and patience. His good advice and support has been invaluable on both an academic and a personal level, for which I am extremely grateful.

I would also like to thank the members of the Haseyama laboratory at Hokkaido University for their help. In particular, I would like to acknowledge the valuable support of Specially Appointed Professor Shigenobu Minami, Assistant Professor Sho Takahashi and Ms. Kahori Kitaichi.

Furthermore, I would like to show my great appreciation to Professor Shoichiro Yamasaki and Professor Tomoko K. Matsushima of Polytechnic University, who gave me valuable comments and very useful knowledge about research.

Finally, I would like to thank my wife Akie who continually supported me in completing this study. This study would not have been possible without her support.